LAWRENCE
LIVERMORE
NATIONAL
LABORATORY

UCRL-JRNL-203889

Experimental Determination of Thermodynamic Properties of Ion-Exchange in Heulandite: Binary Ion-Exchange Experiments at 55 and 85 ºC involving Ca^{2+}, Sr^{2+}, Na^{+}, and K^{+}

Th. Fridriksson, P. S. Neuhoff, B. E. Viani, and D.K. Bird

April 30, 2004

Submitted to American Journal of Science

This work was performed under the auspices of the U.S. Department of Energy by University of California, Lawrence Livermore National Laboratory under Contract W-7405-Eng-48.

Experimental determination of thermodynamic properties of ion-exchange in heulandite: Binary ion-exchange experiments at 55 and 85 ºC involving Ca^{2+}, Sr^{2+}, Na^{+}, and K^{+}

Thráinn Fridriksson,[1,2,*] Philip S. Neuhoff[3], Brian E. Viani[4], and Dennis K. Bird[1]

[1] Department of Geological and Environmental Sciences, Stanford University, Stanford CA 94305-2115, USA

[2] Iceland GeoSurvey, Grensásvegur 9, 108 Reykjavik, Iceland

[3] Department of Geological Sciences, University of Florida, 241 Williamson Hall, P.O. Box 112120, Gainsville, FL 32611-2120, USA

[4] Biogeochemical Dynamics Group, Lawrence Livermore National Laboratory, 7000 East Avenue, PO 808, Livermore, CA 94550

* corresponding author: **thf@isor.is**

_____, tel: 354 528 1532

revised for American Journal of Science

UCRL-JRNL-203889

ABSTRACT. Heulandite is a common rock-forming zeolite that exhibits wide solid solution of extraframework cations, presumably due to ready ion exchange with aqueous solutions. In order to provide a quantitative basis for interpreting and predicting the distribution of aqueous species between heulandite and aqueous solutions, ion exchange equilibrium between heulandite and aqueous solutions with respect to the binary cation pairs Ca^{2+} – K^{+}, Ca^{2+} – Na^{+}, K^{+} – Na^{+}, K^{+} – Sr^{2+}, Na^{+} – Sr^{2+}, and Ca^{2+} – Sr^{2+} was investigated. Homoionic Ca-, K-, and Na-heulandites prepared from natural heulandite were equilibrated with 0.1 N Cl^{-} solutions containing various proportions of the cations in a given binary pair at 55 and 85 °C to define isotherms describing partitioning of the cations over a wide range of heulandite and solution composition with respect to the cations in each pair. In general, the experiments equilibrated rapidly, within 11-15 weeks at 55 °C and 3-4 weeks at 85 °C. The exception was the Ca^{2+} – Sr^{2+} binary exchange, which did not equilibrate even after 3 months at 55 °C and 4 weeks at 85 °C. Slow exchange of Sr^{2+} for Ca^{2+} also prohibited preparation of homoionic Sr-heulandite from the natural (Ca-rich) heulandite within 10 weeks in 2N $SrCl_2$ solution at 90 ºC, although near homoionic Sr-heulandite was produced by exchange of K- and Na-heulandite. Experimentally determined isotherms were used to derive equilibrium constants for the ion exchange reactions and asymmetric Margules models describing the extent of non-ideality in extraframework solid solutions in heulandite. Regressed equilibrium constants for Ca^{2+}-Na^{+}, Ca^{2+}-K^{+}, and K^{+}-Na^{+} binary cation pairs at 55 ºC are internally consistent among each other (complying with the triangle rule), indicating good accuracy of these data. The maximum departure from internal

consistency among the equilibrium constants for three binary pairs was 900 J per mole of charge equivalents (eq) for the 55 ºC experiments and 2300 J eq^{-1} for the 85 ºC experiments. The applicability of the present experimental results and thermodynamic models was assessed by calculating the composition of heulandite in Icelandic geothermal systems from known compositions using the regressed thermodynamic properties of Ca^{2+}-Na^{+} exchange at 85 ºC. Calculations predict an average Ca mole fraction [defined as Ca/(Ca+Na)] in heulandite of 0.74, in excellent agreement with observed compositions of heulandite from geothermal and metamorphic systems in Iceland (0.75). Thermodynamic data for heulandite ion-exchange derived in this study can be used to predict partitioning of Ca, K, Na, and Sr between heulandite and aqueous solutions in geologic systems. Because heulandite is the most effective sink for Sr in basaltic aquifers that have undergone zeolite facies metamorphism, the experimental results of this study will provide essential data for modeling Sr transport in aquifers in low-grade metabasalts.

INTRODUCTION

Natural zeolites are tectosilicates, characterized by silicon and aluminum tetrahedra surrounding ~ 2 to 10 Å wide channels containing molecular water and extraframework cations (c.f., Gottardi and Galli, 1985; Armbruster and Gunter, 2001; Passaglia and Shepard, 2001). The presence of aluminum atoms in tetrahedral sites of a tectosilicate framework results in one charge equivalent (eq) of negative charge of the tetrahedral framework per mole of Al. This negative charge is compensated with the same amount of positive charge of extraframework cations. The open structure of the zeolite

framework and the requirement of net charge balance of the mineral result in high cation-exchange capacities of many zeolites, a property utilized in several industrial systems, for example, for water softening and waste water treatment (c.f., Tsitsishvili, 1988; Kalló, 2001), for agricultural purposes, for example, to enhance fertilizer efficiency and for soil remediation (Ming and Allen, 2001). Natural zeolites commonly form at low temperatures by reactions of aqueous solutions with volcanic rocks and volcanogenic sediments and, consequently, ion-exchange capabilities of zeolites can affect ground water composition and quality in volcanic aquifers (for example White and others, 1980; Sturchio and others, 1989, 1993). For example, the ability of certain zeolite species to preferentially incorporate Sr^{2+} into their crystal structure *via* ion-exchange potentially provides an important sink for radioactive ^{90}Sr (half-life 28 years) derived from transuranic nuclear waste. Ion-exchange reactions that incorporate Sr^{2+} into zeolites, such as the HEU-framework zeolites (clinoptilolite and heulandite) are a potential mechanism for attenuating ^{90}Sr mobility in volcanic aquifers at nuclear waste sites like Hanford Nuclear Reservation, Washington USA (Illman, 1993) and Yucca Mountain, Nevada USA (for example, Broxton and others, 1987; Viani and Bruton, 1992).

The chemical composition of heulandite is described with the general formula $(Ca_{0.5},Sr_{0.5},Ba_{0.5},Mg_{0.5},Na,K)_{2.25}Al_{2.25}Si_{6.75}O_{18}\bullet nH_2O$ (Coombs and others, 1998). The water content, nH_2O, of heulandite in equilibrium with liquid water at 25 ºC and 1 bar is a function of cation content. It ranges from about 5.5 water molecules per 18 framework oxygen atoms (pfu; in this communication pfu refers to a formula unit of 18 framework oxygen atoms) in K-rich heulandite to about 7 water molecules pfu in Ca-rich heulandite (see below). Figure 1 depicts the compositions of clinoptilolite and heulandite in terms

of the fraction of divalent extraframework cations [(Ca^{2+} + Sr^{2+} + Mg^{2+} + Ba^{2+})/(all extraframework cations)] as a function of aluminum content per formula unit of 18 framework oxygen atoms. Clinoptilolite and heulandite are isostructural but are characterized by different Si/Al ratio (Coombs and others, 1998), with heulandite having Si/Al < 4 and clinoptilolite with Si/Al ≥ 4. The distribution of analyses in figure 1 illustrates the continuous solid solution among and between clinoptilolite and heulandite, with respect to both framework composition and extraframework content. While natural samples of both heulandite and clinoptilolite exhibit wide substitution in the extraframework sites, this substitution is typically more extreme in the latter leading to more monovalent cation-rich compositions. Modeling of the stability of these minerals, and the effects of ion exchange between them and aqueous solutions, requires consideration of these substitutions. In the case of clinoptilolite, its widespread occurrence in economic-grade deposits and predominance in the silicic tuff units in Yucca Mountain have led to numerous physico-chemical studies (for example Johnson and others, 1991; Carey and Bish, 1996, 1997; Wilkin and Barnes, 1998, 1999; Benning and others, 2000; Yang and others, 2001; Armbruster, 1993; Smyth and others, 1990; Bish and Carey, 2000), including investigations of ion-exchange properties (for example, Ames, 1964; Pabalan, 1994; Pabalan and Bertetti, 1999; Valcke and others, 1997a,b; White and others, 1999; Palmer and Gunter, 2001; Woods and Gunter, 2001). In contrast, ion-exchange experiments on heulandite are sparse, and the temperature dependence of ion exchange reactions in neither mineral species has received much attention. While both minerals typically form at temperatures of ~ 50 to 110 °C, most ion exchange studies are restricted to 25 °C. Predictive modeling of Sr^{2+} attenuation by these

minerals at *in situ* conditions within the earth's crust requires knowledge of the effects of temperature and framework composition on ion exchange reactions.

The goal of the present study is to provide experimental data and thermodynamic models necessary for predicting the cation-exchange properties of heulandite. The results of binary ion-exchange experiments on natural heulandite involving Ca^{2+}, K^{+}, Na^{+}, and Sr^{2+} at 55 and 85 °C are used to constrain thermodynamic analyses of binary ion-exchange reactions and activity-composition relationships for heulandite. The resulting thermodynamic data can be used to predict heulandite compositions in equilibrium with ground waters and geothermal solutions of known compositions and vice versa at temperatures where heulandite forms in geologic systems. Furthermore, the experimentally determined equilibrium constants for ion-exchange reactions permit calculation of the relative Gibbs energy of formation of homoionic Ca-, K-, Na-, and Sr-heulandites. When coupled with experimental determination of the Gibbs energy of formation of one or more of the homoionic heulandite endmembers, these results facilitate evaluation of the thermodynamic stability of heulandite solid solutions in natural systems for predictive modeling of heulandite parageneses and reactive transport modeling of Sr^{2+} mobility in basaltic aquifers.

EXPERIMENTAL

Sample Characterization

The heulandite used in ion-exchange experiments in this study was a hydrothermal fracture filling in Tertiary basalt lava at Teigarhorn, eastern Iceland (stage III alteration of Neuhoff and others, 1999). The original sample was a fist-sized fragment of the fracture filling that consisted of large (1 to 5 cm) intergrown crystals of heulandite with minor stilbite. The sample was broken up and clear heulandite fragments were handpicked under a binocular microscope. Heulandite is easily separated from stilbite because it is clear and has perfect cleavage whereas stilbite is milky and lacks the perfect cleavage of heulandite. Handpicked heulandite was ground in a SPEX shatterbox using a tungsten carbide vessel and the 2 to 10 μm size fraction used for subsequent ion-exchange experiments was separated by repeated centrifugation. The purity of the heulandite powder was checked by synchrotron X-ray powder diffraction at beamline 2-1 at Stanford Synchrotron Radiation Laboratory. The only exotic reflections observed in the diffraction patterns were consistent with minor stilbite contamination. The amount of stilbite contamination was determined to be less than 0.1% by a standard addition method.

Bulk chemical composition and chemical homogeneity of the natural heulandite was determined by ICP techniques, thermogravimetric analyses and electron microprobe analyses. Major element concentrations of the bulk powder were determined by ICP-AES and the concentrations of Sr and Ba were determined by ICP-MS at a commercial laboratory (ALS-Chemex). The heulandite was prepared for ICP analyses by lithium metaborate fusion and dissolution in 10% HNO_3. Approximately 20 randomly selected

crystal fragments were analyzed by electron microprobe to assess the chemical homogeneity of the natural heulandite.

Bulk composition of the natural heulandite powder determined by ICP-AES is listed in Table 1 in terms of number of atoms pfu and corresponds to $Na_{0.26}K_{0.05}Ca_{0.90}Sr_{0.03}Al_{2.17}Si_{6.78}O_{18}\bullet nH_2O$. The bulk composition of the natural heulandite is also depicted on figure 1 (large solid circle) in terms of the mole fraction of divalent extraframework cations, $X_{M^{2+}}$, as a function of the number of Al atoms per formula unit of 18 framework oxygen atoms. Small solid circles on figure 1 represent electron microprobe analyses of selected crystal fragments of heulandite used in this study. Each circle represents an average of 3 to 6 closely spaced spot analyses from a single crystal fragment. Figure 1 illustrates that the composition of the natural heulandite ranges from 2.11 Al pfu and $X_{M^{2+}}$ equal to ~0.80 to 2.28 Al pfu and $X_{M^{2+}}$ equal to ~0.75. Each set of 3 to 6 closely spaced spot analyses generally exhibited smaller compositional variation than indicated by the size of the shaded round symbols in figure 1. Therefore the distribution of the electron microprobe analyses in figure 1 represents real compositional variation of intergrown heulandite crystals in the natural sample. Figure 1 also depicts compositions of natural heulandite from Icelandic basalts (solid triangles; table 2), natural heulandite (shaded upward pointing triangles) and clinoptilolite (shaded downward pointing triangles) from various geologic settings reported by Alietti and others (1977), and compositions of heulandite and clinoptilolite from Yucca Mountain (small open squares; Bish and Boak, 2001). The composition of the natural clinoptilolite used for ion-exchange experiments by Pabalan (1994) and Pabalan and Bertetti (1999) is shown by a large shaded cirlce. Inspection of figure 1 shows that the

heulandite used in this study has fairly high content of divalent cations (mainly Ca^{2+}) but intermediate to low Al content compared to the range of heulandite compositions reported by Alietti and others (1977).

Homoionic Exchange

Homoionic Na-, Ca-, K-heulandites were prepared by immersing ~1 to 2 g of natural heulandite in 250 g of 2 N chloride solutions of the respective cations. High-density polyethylene (HDPE) bottles containing the powdered heulandite and 2 N chloride solutions were rotated continuously in an oven at 90 °C. The chloride solutions were replaced weekly for 6 to 8 weeks. Finally, the ion-exchanged heulandite powder was washed with deionized water and dried in an oven at 90 °C. The chemical compositions of the homoionic heulandites were determined by ICP-AES and the water content of a fully hydrated homoionic heulandite was determined by heating a powdered sample to 900 °C in a thermogravimetric analysis (TGA) instrument after equilibration at 24.3 °C and 100% relative humidity. Attempts to prepare homoionic Sr-heulandite from the Ca-rich natural heulandite were unsuccessful because of very slow exchange of Sr^{2+} for Ca^{2+}. After 8 weeks at 90 °C in 2N Sr^{2+} solution the natural heulandite had only exchanged ~30% of its original extraframework cations for Sr^{2+}. However, the exchange of Sr^{2+} into homoionic Na- and K-heulandites was much more rapid, and near homoionic Sr-heulandite was produced in binary experiments that used Na- and K-heulandite as starting material (see below).

Table 1 lists the chemical compositions of the homoionic heulandites used in this study. It can be seen from table 1 that none of the nominally homoionic endmembers are

truly homoionic. In all cases other extraframework cations constitute 2.5 to 7% of the total extraframework charge. Incomplete exchange is commonly observed in studies of ion-exchange properties of zeolites, even in zeolites where cation-exchange is much more rapid than in heulandite such as clinoptilolite and phillipsite (c.f. Tsitsishvili and others, 1992 and references therein). For example, K^+, Mg^{2+} and Ca^{2+} amounted to ~10% of the total extraframework charge in the ion-exchanged Na-clinoptilolite used in binary ion-exchange experiments reported by Pabalan (1994) and Pabalan and Bertetti (1999). Similarly, in the Na-exchanged phillipsites used in ion-exchange experiments reported by Shibue (1981, 1998) cations other than Na^+ constituted 3 to 10% of the total extraframework cation charge. Generally, incomplete homoionic exchange is attributed to cations located on crystallographic sites that are inaccessible to exchange due to local crystal defects and it is assumed that these cations do not participate in the ion-exchange process (Pabalan, 1994). This assumption was supported by ICP analyses of selected run products of the binary experiments of this study that demonstrated that even after more than four months equilibration time in binary exchange experiments involving Na^+ and Ca^{2+}, the concentrations of K^+ and Sr^{2+} in the solid were not significantly lower that in the homoionic Na- and Ca-heulandites listed in table 1.

The effect of exchange to homoionic endmembers on the tetrahedral framework of heulandite was assessed using ^{29}Si magic angle spinning nuclear magnetic resonance (MAS NMR) spectroscopy performed on a modified Varian VXR/Unity-400S spectrometer with a 9.4 Tesla (T) magnet (79.46 MHz for ^{29}Si). The spectra were referenced to external tetramethyl silane. Each spectrum exhibited four main signals at approximately –95 ppm, -100 ppm, -105 ppm and –111 ppm similar to previous studies

of heulandite and clinoptilolite (for example, Ward and McKague, 1994; Kato and others, 1997). As discussed by Kato and others (1997), these signals are probably composites of individual signals arising from differing proportions of next-nearest neighbor Si and Al around the five distinct tetrahedral sites in heulandite. The composite nature of these signals leads to ambiguities in line shape and prevents unambiguous assignment to specific sites and next-nearest neighbor configurations. Nonetheless, visual comparison and semi-quantitative fitting of the spectra suggests that no significant modifications to the heulandite framework occurred other than distortions of the framework (apparent as < 2 ppm differences in the chemical shifts). The relative abundances of the signals are virtually the same between the natural heulandite starting material and the homoionic endmembers, indicating that the Si-Al ordering state and the framework composition remained unchanged (as indicated by the chemical analyses in table 1).

Binary Ion-Exchange Experiments

There are six possible binary combinations of the four cations considered in this study, that is Ca-Sr, K-Ca, K-Na, K- Sr, Na-Ca, and Na-Sr. Ion-exchange isotherms for all these binaries were measured at 55.0 ± 1.0 and 85.0 ± 1.0 ºC, with the exception of Ca-Sr where equilibrium was not attained within the duration of our experiments due to slow exchange kinetics. Each binary ion-exchange isotherm consisted of 10 to 27 individual exchange experiments where the equilibrium partitioning of the two cations between the heulandite and the coexisting aqueous solution was determined. The experimental approach is described below for a general binary system containing the cations A^{a+} and B^{b+} where a+ and b+ refer to the charge of the cations.

Individual binary ion-exchange experiments were set up by combining homoionic heulandite containing either A or B with an aqueous solution that contained the two cations in a known ratio. Ion-exchange isotherms where A-heulandite was used as starting material were referred to as A/B isotherms and vice versa (A/B isotherms determined at 55 and 85 °C are referred to as A/B 55 and A/B 85, respectively). The setup of each exchange experiment involved weighing homoionic heulandite powder into an empty HDPE bottle and then adding measured amounts of 0.1 N ACl_a and BCl_b stock solutions. The amounts of heulandite and the two stock solutions were varied for the 10 to 27 individual exchange experiments of each isotherm so that the ratio of A:B in the system (aqueous solution and heulandite powder) ranged from 1000 to 0.005 for a given isotherm. The stock solutions were prepared using reagent grade NaCl, KCl, $CaCl_2 \cdot 2H_2O$, and $SrCl_2 \cdot 6H_2O$ and MegaPure® de-ionized water. In general between ~40 to ~70 ± 1 mg of heulandite were used for individual ion-exchange experiments and the total amount of solution generally ranged between 15 and 30 ± 0.002 g. However, in some cases it was necessary to use smaller amounts of heulandite (down to 10 mg) and larger amounts of solution (up to 250 g) to achieve complete ion-exchange (that is obtain B-heulandite in an A/B experiment). The final step in the preparation of the experiments was to weigh each bottle containing heulandite powder and experimental solution. The initial weight measurement was used along with the measured weight at the end of the experiment to account for any weight loss of the individual exchange experiments during equilibration due to evaporative water loss at the experimental temperature as explained below.

HDPE bottles containing heulandite powder and experimental solutions were placed in a VWR horizontal airflow oven equipped with a Watlow temperature controller that maintained constant temperature within ± 1.0 ºC. In order to prevent excess pressure in the bottles caused by increased vapor pressure of water and thermal expansion of the contents of the HDPE bottles (experimental solution and air in headspace) due to the heating from room temperature to 55 and 85 ºC, the experimental solutions were allowed to thermally equilibrate in their bottles for ~30 minutes at the experimental temperature before they were tightly closed. The bottles were either rotated continuously in the oven in order to facilitate mixing of the heulandite powder with the aqueous solution or shaken by hand at least once a day. The exchange experiments were allowed to equilibrate for 11 to 15 weeks at 55 °C and 3 to 4 weeks at 85 °C.

At the end of each experiment the bottles containing heulandite and the experimental solution were weighed. The experimental solutions were separated from the heulandite powder by filtration through a 0.2-µm pore-size filter, and promptly sealed off and refrigerated. The heulandite powder left on the filter was washed by rapidly passing ~1 liter of de-ionized water through the sample on the filter. The rinsed heulandite powder from each experiment was washed off the filter into a Petri dish, dried, and stored.

The concentrations of A^{a+} and B^{b+} in the equilibrated experimental solutions were determined by ICP-AES analyses after 1:10 dilution with de-ionized water. Standards were prepared from commercial standard solutions containing 1000 ppm of A^{a+} and B^{b+} in 1% HCl. Because the concentration ratios of A^{a+} to B^{b+} in the experimental solutions of each exchange isotherm varied greatly (from 1:1000 to 1000:1) it was necessary to

prepare two standards for the analyses of each set of binary experimental solutions (that is, each isotherm). A 'high-A standard' had concentration of A^{a+} similar to the expected concentration of A^{a+} in the most A-rich experimental solutions after the 1:10 dilution (~100 ppm for Ca and Na, and ~220 for K and Sr), and with a concentration of B ~20% of that concentration. A corresponding 'high-B standard' was prepared. All experimental solutions for each isotherm were analyzed using both standards. The agreement between the analyses using the different standards was generally good at intermediate A:B ratios, and in those cases the concentrations of these cations in the experimental solutions were taken to be equal to the average of the two determinations. However, near the compositional extrema of the isotherms one determination was used; that is, at the high A:B end of the isotherm only the compositions determined using the high-A standard were used, and vice versa for the low A:B end of the isotherm.

The cation composition of the heulandite after equilibration with the experimental solution in each ion-exchange experiment was calculated from observed changes of the concentrations of A^{a+} and B^{b+} in the experimental solution during the course of the experiment. This approach is similar to the 'conservation of mass' approach used by Pabalan (1994) and Pabalan and Bertetti (1999, 2001) but is modified to account for the effects of minor loss of water from the HDPE bottles in our experiments (see Results section). For an exchange experiment starting with a homoionic A-heulandite (that is an A/B experiment), the final B content of the heulandite in terms of number of moles of B pfu, $\bar{n}_{\mathrm{B}}^{\mathrm{final}}$, is calculated by

$$\bar{n}_{\mathrm{B}}^{\mathrm{final}} = \left(m_{\mathrm{B,stock}}\, wt_{\mathrm{B-stock}} - m_{\mathrm{B}}^{\mathrm{final}}\, wt_{\mathrm{solution}}^{\mathrm{final}}\right)\frac{FW_{\mathrm{A-heul}}}{wt_{\mathrm{A-heul}}} \qquad (1)$$

where $m_{\mathrm{B,stock}}$ and $m_{\mathrm{B}}^{\mathrm{final}}$ represent the molal concentrations of B^{b+} in the B-stock solution and in the final solution after equilibration, $wt_{\mathrm{B\text{-}stock}}$ refers to the amount of the B-stock solution in the initial system, $wt_{\mathrm{solution}}^{\mathrm{final}}$ refers to the total amount of solution in the HDPE bottle at the end of the experiment, $FW_{\mathrm{A\text{-}heul}}$ refers to the formula weight of A-heulandite per 18 framework O atoms, and $wt_{\mathrm{A\text{-}heul}}$ refers to the weight of A-heulandite in the initial system. The final amount of solution is equal to the sum of the two stock solutions minus the weight loss, or

$$wt_{\mathrm{solution}}^{\mathrm{final}} = wt_{\mathrm{A-stock}} + wt_{\mathrm{B-stock}} - \left(wt_{\mathrm{total}}^{\mathrm{initial}} - wt_{\mathrm{total}}^{\mathrm{final}}\right), \qquad (2)$$

where $wt_{\mathrm{A-stock}}$ is the initial weight of the A^{a+} stock solution and $wt_{\mathrm{total}}^{\mathrm{initial}}$ and $wt_{\mathrm{total}}^{\mathrm{final}}$ refer to the initial and final weights of the experimental system (that is the HDPE bottle containing the solution and heulandite). The number of moles of A in a formula unit of heulandite after equilibration, $\bar{n}_{\mathrm{A}}^{\mathrm{final}}$, in an A/B exchange experiment is calculated by

$$\bar{n}_{\mathrm{A}}^{\mathrm{final}} = \left(\frac{CEC_{\mathrm{A}}\, wt_{\mathrm{A-heul}}}{\mathrm{a}} - m_{\mathrm{A,stock}}\, wt_{\mathrm{A-stock}} - m_{\mathrm{A}}^{\mathrm{final}}\, wt_{\mathrm{solution}}^{\mathrm{final}}\right)\frac{FW_{\mathrm{A-heul}}}{wt_{\mathrm{A-heul}}}. \qquad (3)$$

The cation-exchange capacity of heulandite for A^{a+} (CEC_{A}) is defined as

$$CEC_{\mathrm{A}} = \frac{\mathrm{a}\bar{n}_{\mathrm{A,hom\,oionic}}}{FW_{\mathrm{A\text{-}heul}}}, \qquad (4)$$

where $\bar{n}_{\mathrm{A,hom\,oionic}}$ represents the number of A^{a+} per formula unit of A-heulandite. In addition to calculating the final compositions of the heulandite by the above 'conservation of mass'-method the final compositions of the heulandite from 1 to 15 individual exchange experiments from each of the binary isotherms were analyzed independently by ICP-AES. The number of heulandite samples from a given isotherm analyzed by ICP-AES depended on the scatter of the calculated heulandite compositions

(see below). For isotherms that exhibited little scatter (for example Ca/Na 55, Na/Ca 55, K/Ca 55, K/Sr 55, and K/Sr 85) only one to three solid samples were analyzed, whereas for isotherms where scatter of the computed heulandite compositions prevented the determination of the isotherm topology (for example K/Na 55, Na/Sr 55, Na/Sr 85, Ca/K 85, K/Ca 85, Na/Ca 85, and Na/K 85) a larger number of solid phase analyses was necessary. Furthermore, some of the binary exchange isotherms were reversed, that is, both A/B and B/A isotherms were determined, in order to demonstrate reversibility of the ion-exchange reactions.

The extent of sample dissolution and potential recrystallization of the heulandite powder was evaluated by ICP analyses of experimental solutions, scanning electron microscopy (SEM) and X-ray diffraction (XRD) on selected run products from binary ion-exchange experiments in addition to the ^{29}Si MAS NMR experiments on the homoionic Ca-, K-, and Na-heulandites. Figure 2A depicts an SEM image showing a part of a typical untreated heulandite grain and figure 2B shows a typical heulandite grain that has undergone ion-exchange (from the Na/Sr 85 23 experiment, 8 weeks at 90 °C in a 2 N NaCl solution and 3 weeks at 85°C in a 0.1 N Sr solution). The edges of the exchanged grain are clearly more rounded than the very sharp edges of the untreated grain, indicating some dissolution of the sample during the experiment. However, the overall angularity of the exchanged grain and small crystal fragments that are still present on the surface of the ion-exchanged grain suggest that dissolution was not very extensive. Silica concentrations in selected experimental solutions from the 85 °C experiments ranged between 0.07 and 0.28 mmol/kg with an average of 0.16 mmol/kg. For a typical binary exchange experiment consisting of ~30 ml of solution and 50 mg of heulandite,

0.16 mmol/kg of dissolved silica corresponds to ~1% of the silica in the system. However, several experiments had larger volumes of solution (~60 ml) and smaller amounts of heulandite (down to ~10 mg) and in those cases 0.16 mmol/kg of dissolved silica corresponds to ~10% of the silica in the system. Comparison of detailed XRD patterns of the homoionic Ca-, Na-, and K-heulandites and of selected run products did not indicate the presence of exotic reflections in the run products, suggesting that new phases did not form in the heulandite powder during the experiments. As noted above, ^{29}Si MAS NMR spectra for the homoionic Ca-, K-, and Na-heulandites and the natural heulandite indicated that the ion-exchange did not result in changes of the Si/Al ordering state of the heulandite framework nor in changes of the Si/Al ratio of the framework. The absence of detectable amounts of secondary phases suggests that the dissolved silica concentration can be taken as a proxy for the total dissolution of heulandite during the experiment. In that case, dissolution of 1% of the experimental heulandite in a typical exchange experiment (30 ml solution, 50 mg heulandite) would result in the release of ~0.05 meq/kg of extraframework cations, which is insignificant in comparison to the total cation concentration of the experimental solutions (100 meq/kg) and is much smaller than the analytical error on the fluid analyses (see below).

RESULTS

Tables 3 to 14 list the results of the binary ion-exchange experiments along with pertinent experimental details. The results in tables 3 to 14 include the concentrations of both cations in final experimental solution, and the ratio of the two cations in coexisting heulandite, reported as mole fraction of one of the cations, defined as

$$X_A = \frac{\bar{n}_A}{\bar{n}_A + \bar{n}_B}. \quad (5)$$

The mole fraction of the other cation in the binary pair, X_B, is calculated by

$$X_B = 1 - X_A. \quad (6)$$

Tables 3 to 14 list both solid phase mole fractions computed from the fluid composition using equations (1) and (3) as well as solid phase mole fractions determined directly by ICP-AES. The observed weight loss of the experimental system during equilibration at the experimental temperature is also reported in tables 3 to 14. Experimental details listed in tables 3 to 14 include the duration of the experiments, amount of homoionic heulandite used, and the amounts used of the A- and B-stock solutions.

Some of HDPE bottles showed unambiguous signs of leakage at 85 °C, that is, salt precipitation on the outer surface of the bottles and considerable, even complete, loss of fluid. In those cases the experiments were discarded and excluded from further analyses. However, the weight of all HDPE bottles containing individual ion-exchange experiments decreased uniformly during the experiments without any signs of fluid leakage. The most severe weight loss was experienced by the longest-running ion-exchange experiments, that is, those of the Na/Ca isotherm at 55 °C where the average weight loss was 4.6 ± 0.8%. For all other isotherms at 55 and 85 °C the average weight loss was between 1.5 ± 0.2 and 3.5 ± 0.5%. We concluded that the uniform weight loss was a result of H_2O vapor diffusion through the walls of the HDPE bottles based on the uniformity of the weight loss and the absence of salt precipitation on the outside of the bottle. The general increase in the total cation concentration of the experimental solutions during the experiments also supports our conclusion that only H_2O (that is no electrolytes or heulandite) was lost from the HDPE bottles.

The average relative errors on the ICP-AES determinations of the cation concentrations (defined as two times the standard deviation of three analyses divided by the average of the three analyses) of experimental solutions were between 2 and 4%. However, the nature of our experimental system allows independent evaluation of the quality of the ICP analyses by comparing the total normality of the experimental solutions calculated from the ICP analyses, $N_{\text{total}}^{\text{final,ICP}}$, to the total normality calculated from the initial normality of the solution and the observed weight loss, $N_{\text{total}}^{\text{final,wt-corr}}$. The total normality of the solution based on the ICP results is calculated by

$$N_{\text{total}}^{\text{final,ICP}} = \text{a}m_{\text{A}}^{\text{final,ICP}} + \text{b}m_{\text{B}}^{\text{final,ICP}}, \tag{7}$$

where $m_{\text{A}}^{\text{final,ICP}}$ and $m_{\text{B}}^{\text{final,ICP}}$ are the molal concentrations of A^{a+} and B^{b+} in the final experimental solutions, respectively, as analyzed by ICP. Assuming that the observed weight loss represents loss of pure H_2O vapor from the HDPE bottles, that is, the number of cations in the experimental system is conserved, the calculated total normality of the final solution based on the initial normality of the experimental solution and the observed weight loss is

$$N_{\text{total}}^{\text{final,wt-corr}} = N_{\text{total}}^{\text{initial}} \frac{wt_{\text{solution}}^{\text{initial}}}{wt_{\text{solution}}^{\text{final}}}, \tag{8}$$

where $N_{\text{total}}^{\text{initial}}$ is the initial normality of the experimental solution, given by

$$N_{\text{total}}^{\text{initial}} = \frac{N_{\text{A-stock}} wt_{\text{A-stock}} + N_{\text{B-stock}} wt_{\text{B-stock}}}{wt_{\text{solution}}^{\text{initial}}}. \tag{9}$$

Because $N_{\text{total}}^{\text{final,wt-corr}}$ is calculated from relatively accurate and precise weight measurements, it is taken to be more accurate than $N_{\text{total}}^{\text{final,ICP}}$. In general, $N_{\text{total}}^{\text{final,ICP}}$ is very

close to $N_{\text{total}}^{\text{final,wt-corr}}$. The average percent difference (± standard deviation) between $N_{\text{total}}^{\text{final,ICP}}$ and $N_{\text{total}}^{\text{final,wt-corr}}$ for the Na/Sr, K/Na, Na/Ca, Ca/Na, K/Ca, and K/Sr isotherms at 55 °C was –0.1 ± 3.0%, 0.2 ± 2.3%, 0.2 ± 1.4%, 0.9 ± 1.2%, 1.4 ± 2.0%, and 2.2 ± 1.7%, respectively. The corresponding values for the 85 °C isotherms are -5.7 ± 4.0%, 0.5 ± 0.9%, 1.0 ± 2.7%, 1.1 ± 1.4%, 2.5 ± 4.0%, and 3.6 ± 1.7% for the Ca/K, Na/K, Na/Sr, K/Sr, K/Ca and Na/Ca isotherms, respectively.

Despite the relatively good agreement between $N_{\text{total}}^{\text{final,ICP}}$ and $N_{\text{total}}^{\text{final,wt-corr}}$ we found that the random error in the ICP analyses prevented direct use of the uncorrected ICP-concentrations of A^{a+} and B^{b+} for calculation of the cation composition of the heulandite by equations (1) and (3). This is because the cation content of the solid phase, as calculated by equations (1) and (3), is a small difference between two large numbers (the initial and final amounts of the given cation in the solution), so that the relatively small error of solution composition is transferred directly to the error of the much smaller amount of the cation in the solid phase. Thus, calculations of the cation content of the heulandite using equations (1) and (3) and the uncorrected ICP analyses of the concentrations of A^{a+} and B^{b+} in the aqueous solution resulted, in some cases, in unrealistic values, for example, negative concentration values for the solid phase and unacceptable scatter in the resulting exchange isotherms. This problem was largely mitigated by normalizing the aqueous concentrations of A^{a+} and B^{b+} to the expected total normality of the experimental solution, $N_{\text{total}}^{\text{final,wt-corr}}$, calculated by equation (8). The weight correction normalized concentrations of A^{a+} and B^{b+}, $m_{\text{A}}^{\text{wt-corr}}$ and $m_{\text{B}}^{\text{wt-corr}}$, are calculated by

$$m_{\mathrm{A}}^{\mathrm{wt-corr}} = m_{\mathrm{A}}^{\mathrm{ICP}} \frac{N_{\mathrm{total}}^{\mathrm{final,wt-corr}}}{N_{\mathrm{total}}^{\mathrm{final-ICP}}} \text{ and } m_{\mathrm{B}}^{\mathrm{wt-corr}} = m_{\mathrm{B}}^{\mathrm{ICP}} \frac{N_{\mathrm{total}}^{\mathrm{final,wt-corr}}}{N_{\mathrm{total}}^{\mathrm{final-ICP}}}. \qquad (10a,b)$$

The weight correction resulted in only small changes of the cation concentrations of the aqueous solutions. The maximum average correction was 3.6% for the Na/Ca 85 isotherm and the correction was generally less than 2% for the other isotherms (see above). The cation ratios in the aqueous solution are not affected by this correction.

Figures 3 to 12 depict the results of the ion-exchange experiments as exchange isotherms showing the compositions of coexisting heulandite and aqueous solutions. Ion-exchange isotherms are traditionally presented in terms of equivalent fractions of one of the cations in the solid phase as a function of the equivalent fraction of the same cation in the coexisting aqueous phase. The equivalent fraction of A^{a+} in the solid phase ($\overline{E}_{A^{a+}}$) is defined as

$$\overline{E}_{\mathrm{A}} = \frac{\mathrm{a}\overline{n}_{\mathrm{A}}^{\mathrm{final}}}{\mathrm{a}\overline{n}_{\mathrm{A}}^{\mathrm{final}} + \mathrm{b}\overline{n}_{\mathrm{B}}^{\mathrm{final}}}, \qquad (11)$$

and similarly, the equivalent fraction of A^{a+} in the aqueous phase ($E_{A^{a+}}$) is defined as

$$E_{\mathrm{A}} = \frac{\mathrm{a}m_{\mathrm{A}}}{\mathrm{a}m_{\mathrm{A}} + \mathrm{b}m_{\mathrm{B}}}. \qquad (12a)$$

It can be seen from equations (11) and (12) that for a binary system involving A^{a+} and B^{b+} that $\overline{E}_{B^{b+}} = 1 - \overline{E}_{A^{a+}}$ and $E_{B^{b+}} = 1 - E_{A^{a+}}$. It can also be seen by comparing equations (5) and (11) that when both cations in the binary pair have the same charge the equivalent fraction, *E*, is equal to mole fraction, *X*. For heterovalent exchange involving A^{a+} and B^{b+}, the mole fractions reported in tables 3 to 14 are readily converted to equivalent fractions by

$$\overline{E}_A = \frac{aX_A}{aX_A + bX_B} \text{ and } \overline{E}_B = \frac{bX_B}{aX_A + bX_B}. \quad (12b,c)$$

The error bars on the data points in figures 3 to 12 represent estimated uncertainties on the measured fluid compositions and the calculated solid phase compositions. As noted above the relative error on the fluid analyses was taken to equal to two times the standard deviation of three ICP analyses divided by the average value. The uncertainty on the solid phase compositions was estimated by standard error propagation calculations (Nordstrom and Munoz, 1994) as the square roots of the sum of squares of errors of the parameters in equations (1), (2), (3), (4), (10), and (11) (c.f. Pabalan, 1994; Pabalan and Bertetti, 2001).

The shaded symbols (circles and squares) in figures 3 to 12 represent data points where the solid phase equivalent fraction was calculated from computed solid phase compositions using equations (1) and (3) and the fluid phase composition corrected by equation (10a,b). Large solid symbols on these figures represent data points where the solid phase composition was determined directly by ICP-AES analyses, and the open symbols represent the computed solid phase compositions of samples that were also analyzed by ICP-AES. It can be seen from these figures that the topology of several of the binary exchange isotherms is well constrained by the calculated solid phase compositions. This applies to the Ca/Na 55 and Na/Ca 55, K/Ca 55, K/Sr 55, and K/Sr 85 isotherms depicted in figures 3, 4, 6, and 9, respectively. The good agreement between the computed solid phase compositions and solid phase compositions determined by ICP-AES analyses of 1 to 3 selected samples from these isotherms indicates that the calculated solid phase compositions are accurately determined for these isotherms despite relatively large error bars on solid phase compositions. However, the

calculated solid phase compositions of some of the isotherms, including K/Na 55, Na/Sr 55, Ca/K 85 and K/Ca 85, Na/Ca 85, Na/K 85, and Na/Sr 85 (Figs. 5, 7, 8, 10, 11, and 12) exhibited extensive scatter that prevented meaningful thermodynamic analyses of the results. In these cases a larger number of solid phase analyses (up to 13) were necessary to constrain the isotherm topology.

Figure 13 depicting the results of the Ca/Sr 55 and Ca/Sr 85 ion-exchange experiments, illustrates the incomplete exchange of these cations over the duration of the experiments. Inspection of figure 13 shows the maximum Sr uptake of the heulandite was only ~20% after the Ca-heulandite had been exposed to nearly pure $SrCl_2$ solution for 83 days at 55 °C, and that after 25 days at 85 °C only 15 to 20% exchange had occurred. Unfortunately, it was not possible to allow longer equilibration times at these temperatures because of the weight loss of all experiments with time and also because a significant number of the bottles were showing signs of breakage after 3 to 4 weeks at 85 °C.

Two exchange isotherms were successfully reversed. The Ca – Na exchange equilibria at 55 °C (fig. 3, tables 3 and 4) was determined by experiments starting with both Ca-heulandite (Ca/Na 55) and Na-heulandite (Na/Ca 55) and the Ca – K exchange isotherm at 85 °C (fig. 8, tables 9 and 10) was determined by experiments starting with both Ca heulandite (Ca/K 85) and K-heulandite (K/Ca 85). The excellent agreement of the Ca/Na 55 and Na/Ca 55 isotherms, shown in figure 3 illustrates reversibility of the Ca – Na exchange equilibria over the duration of these experiments. Similarly, agreement between the Ca/K 85 and K/Ca 85 isotherms shown in figure 8 demonstrates the reversibility of the Ca – K exchange at 85 °C (note the reversibility is apparent from the

data points depicting the analyzed solid phase compositions). Other isotherms were not reversed. However, inspection of figures 3 to 13 reveals that for all A/B isotherms (with the exception of the Ca – Sr isotherms, see above) the composition of the pure B-heulandite endmember is approached. This observation suggests that since there was enough time for complete ion-exchange of heulandite at the compositional extrema of the isotherms the compositionally intermediate experiments must have had sufficient time to reach equilibrium as well. Therefore, with the exception of the Ca – Sr isotherms all the ion-exchange isotherms shown in figures 3 to 13 are assumed to represent equilibrium exchange isotherms.

THERMODYNAMIC ANALYSIS

The thermodynamic analyses of our experimental results are based on the approach outlined by Pabalan (1994) and Pabalan and Bertetti (1999, 2001) with the addition of explicit account for the water stoichiometry of ion-exchange reactions. According to the Vanselow convention for ion-exchange reactions (Vanselow, 1932; Argersinger and others, 1950) a general exchange reaction between A^{a+} and B^{b+} can be expressed as

$$aB^{b+} + bAZ_a \cdot an_A H_2O = bA^{a+} + aBZ_b \cdot bn_B H_2O + ab(n_A - n_B)\, H_2O, \qquad (13)$$

where Z refers to one charge equivalent of the alumino-silicate framework (this corresponds to 1:2.17 part of a formula unit for the heulandite used in this study) and n_A and n_B refer to number of water molecules per one charge equivalent of the heulandite framework of the homoionic zeolite at a given temperature. The standard state adopted for the aqueous species is that of unit activity of a hypothetical one molar solution referenced to infinite dilution and the standard state for the solid phase is unit activity of

the homoionic endmembers in equilibrium with an infinitely dilute aqueous solution of their respective cations (Gaines and Thomas, 1953) at any temperature and pressure. Note that this solid phase standard state implies equilibrium between the zeolite and liquid water.

The equilibrium constant for reaction (13) is

$$K_{(A/B)} = \frac{(m_{A^{a+}}\gamma_{A^{a+}})^{b}(a_{H_2O})^{ab(n_A-n_B)}(X_B\lambda_B)^{a}}{(m_{B^{b+}}\gamma_{B^{b+}})^{a}(X_A\lambda_A)^{b}}, \qquad (14)$$

where a_{H_2O} refers to the activity of water, which can be taken to be equal to unity in the relatively dilute experimental solutions of this study, γ refers to the activity coefficient of the subscripted aqueous cation, and λ_A and λ_B refer to the solid phase activity coefficients of the A- and B-homoionic endmember of the binary A-B solid solution in heulandite. Note that $m_{A^{a+}}$ and $m_{B^{b+}}$ in equation (14) refer to the molalities of the *free* ions of A^{a+} and B^{b+} in aqueous solution and should not be confused with the *total* molalities of these ions (m_A and m_B) in solution as determined by chemical analyses (see tables 3 to 14). The free ion molalities and activity coefficients for the aqueous species were computed from the measured total molalities of these cations in the experimental solutions, listed in tables 3 to 14 using the EQ3nr aqueous speciation software (Wolery, 1991) and the slop98 upgrade to the SUPCRT92 database (Johnson and others 1992) for thermodynamic properties of aqueous species. Aqueous activity coefficients were calculated using the b-dot extended Debye-Huckel equation. The speciation calculations indicated that 2.4 to 4.4% of the total amount of Sr^{2+} and Ca^{2+} in solution and 1.1 to 1.6% of the total amount of Na^{+} in solution are bound as chloride complexes in the

experimental solutions. Less than 0.03% of the K^+ is bound as chloride complexes in the experimental solutions.

A Vanselow coefficient (k_v), containing all the terms of equation (14) that can be measured by chemical analysis or calculated from solution compositions is defined as

$$k_{v(A/B)} = \frac{(m_{A^{a+}} ?_{A^{a+}})^b (a_{H_2O})^{ab(n_A - n_B)} X_B^a}{(m_{B^{b+}} ?_{B^{b+}})^a X_A^b}. \quad (15)$$

Combining equations (14) and (15) allows the natural logarithm of the equilibrium constant for reaction (13) to be written as

$$\ln K_{(A/B)} = \ln k_{v(A/B)} + a \ln \lambda_B - b \ln \lambda_A. \quad (16)$$

We use a simple subregular Margules formulation to describe the observed nonideality of the heulandite solid solution although other modeling approaches, such as the multiple ideal sites model of Viani and Bruton (1992) may be more appropriate. However, despite the vast number of recent studies that have greatly elucidated the extra framework cation site distribution in HEU group minerals, we feel that a multiple site activity model requires more detailed crystallographic data on cation site occupancies along binary solid solutions in heulandite than are currently available. The applicability of a subregular Margules formulation to model the non-ideality of binary solid solutions in zeolites has been demonstrated by Pabalan (1994) and subsequent studies (Shibue, 1998; Pabalan and Bertetti, 1999, 2001). The Margules formulation of the natural logarithm of the solid phase activity coefficients in an asymmetric, binary solid solution between homoionic A- and B-heulandites are expressed as

$$\ln \lambda_A = \frac{X_B^2 (W_{A-B} + 2X_A (W_{B-A} - W_{A-B}))}{RT} \quad (17a)$$

and

$$\ln \lambda_{\mathrm{B}} = \frac{X_{\mathrm{A}}^{2}(W_{\mathrm{B-A}} + 2X_{\mathrm{B}}(W_{\mathrm{A-B}} - W_{\mathrm{B-A}}))}{\mathrm{R}T}, \qquad (17b)$$

where $W_{\mathrm{A\text{-}B}}$ and $W_{\mathrm{B\text{-}A}}$ are binary Margules interaction parameters, R is the gas constant and T is temperature in Kelvin (Saxena, 1973; Anderson and Crerar, 1993).

Substitution of equations (17a,b) into equation (16) yields

$$\ln k_{\mathrm{v(A/B)}} = \ln K_{\mathrm{(A/B)}} - \mathrm{a}\frac{X_{\mathrm{A}}^{2}(W_{\mathrm{B-A}} + 2X_{\mathrm{B}}(W_{\mathrm{A-B}} - W_{\mathrm{B-A}}))}{\mathrm{R}T} + \mathrm{b}\frac{X_{\mathrm{B}}^{2}(W_{\mathrm{A-B}} + 2X_{\mathrm{A}}(W_{\mathrm{B-A}} - W_{\mathrm{A-B}}))}{\mathrm{R}T}. \qquad (18)$$

Nonlinear regression of equation (18) to experimentally determined values of $k_{\mathrm{v(A/B)}}$ as a function of mole fraction of A and B allows determination of $\ln K_{\mathrm{(A/B)}}$, $W_{\mathrm{A\text{-}B}}$, and $W_{\mathrm{B\text{-}A}}$ (cf. Pabalan, 1994). Figures 14 and 15 show the results of the Ca/Na55 and Na/Ca55 experiments and the results of the Na/Ca85 experiments in terms of calculated values of $\ln k_{\mathrm{v(A/B)}}$ for individual ion-exchange experiments as a function of solid phase composition. The error bars on X in figures 14 and 15 were calculated by the same method as for equivalent fractions (E) in figures 3 to 13, that is as square roots of the sum of squared errors through equations (1), (2), (3), (4), and (5) (Pabalan, 1994; Pabalan and Bertetti, 2001). The error on k_{v} was calculated by the same method, and the error on $\ln k_{\mathrm{v}}$ for individual data points depicted in figures 14 and 15 were taken to be equal to the estimated error of k_{v} divided by k_{v} (see Pabalan and Bertetti, 2001). In the regression individual data points were inversely weighted by the combined relative error on k_{v} and X. Note that the open symbols in figures 3 to 12 represent the computed solid phase compositions of experimental heulandite that were also analyzed by ICP (solid symbols). In those cases, only the data that represent analyzed solid phase composition were included in the regression and the data shown by the open symbols on figures 3 and 10

are not depicted on figures 14 and 15. The solid curves in figures 14 and 15 were computed from the regressed values of $\ln K_{(A/B)}$, $W_{A\text{-}B}$, and $W_{B\text{-}A}$ for that isotherm and equation (18). The resulting values for $\ln K_{(A/B)}$, $W_{A\text{-}B}$, and $W_{B\text{-}A}$ for all the equilibrium exchange isotherms determined in this study are listed in table 15 along with the corresponding ion-exchange reaction. The solid ion-exchange isotherm curves in figures 3 to 12 were computed from the regressed values of $\ln K_{(A/B)}$, $W_{A\text{-}B}$, and $W_{B\text{-}A}$ for the respective isotherm, assuming a total aqueous solution normality equal to 0.1 N and using the b-dot extended Debye-Huckel equation to compute activity coefficients for aqueous species.

DISCUSSION

Internal Consistency of Thermodynamic Data

The quality of the regressed thermodynamic data for the ion-exchange reactions in table 15 is readily evaluated by considering the internal consistency of the equilibrium constants for the reactions. For a general, internally consistent, ion-exchange system involving the cations A^{a+}, B^{b+}, and C^{c+}, the equilibrium constant for the A/C exchange reaction must be equal to the product of the equilibrium constants for the A/B and the B/C exchange reactions. This requirement of internal consistency of ion-exchange equilibrium constants is referred to as the “triangle rule” in ion-exchange literature.

Application of the triangle rule allows calculation of the equilibrium constant for the K/Na exchange reaction ($K_{K/Na}$) from the equilibrium constants for both the Ca/Na and K/Ca exchange reactions and the Na/Sr and K/Sr reactions given in table 15. The value for $\ln K_{K/Na\text{-}55}$ calculated from the equilibrium constants for Ca/Na 55 and K/Ca 55

given in table 15 is equal to –2.13 ± 0.14. The excellent agreement of this value with the experimentally determined value for $\ln K_{K/Na-55}$, -2.11 ± 0.55, indicates that the thermodynamic data for Ca/Na, K/Ca, and K/Na exchange at 55 °C are internally consistent. The corresponding value for $\ln K_{K/Na-55}$ calculated from the equilibrium constants for Na/Sr 55 and K/Sr 55, equal to –1.78 ± 0.1, is less negative than the experimentally determined value. The agreement between experimental and calculated values for $\ln K_{K/Na}$ is not as good for the 85 °C data. The experimentally determined value of $\ln K_{K/Na-85}$, equal to –2.53 ± 0.1 is more negative than the calculated values for $\ln K_{K/Na-85}$, equal to –2.07 ± 0.13 and –1.75 ± 0.23, (calculated from the equilibrium constants of the Ca/K 85 and Na/Ca 85, and the K/Sr 85 and Na/Sr 85 exchange reactions, respectively). However, the discrepancy between the experimental value for $\ln K_{K/Na-55}$ and the value calculated from the equilibrium constants for Na/Sr 55 and K/Sr 55 amounts to only 900 J per charge equivalent or 2 kJ per mol of heulandite with a formula unit of 18 framework oxygen atoms (note that a heulandite formula unit of 18 framework oxygen atoms contains 2.17 charge equivalents of extraframework cations). Similarly, the discrepancy between the experimentally determined value for $\ln K_{K/Na-85}$ and the value for $\ln K_{K/Na-85}$ calculated from the equilibrium constants for the K/Sr 85 and Na/Sr 85 exchange reactions amounts to 2.3 kJ eq^{-1} or 5 kJ pfu. These inconsistencies indicate that the errors on the regressed equilibrium constants in table 15 are underestimated. The maximum discrepancy between the regressed equilibrium constants in table 15, 5 kJ pfu, is, nevertheless, smaller than typical errors on experimentally determined standard Gibbs energies of formation for zeolites. For instance, the errors on the two available calorimetric determinations of the Gibbs energy of formation of natural heulandite are

equal to ~10.2 and ~8.6 kJ pfu (Johnson and others, 1985; Kiseleva and others, 2001). This suggests that the thermodynamic data in table 15 can be used, in combination with an experimentally determined value of the Gibbs energy of formation for one or more of the homoionic endmembers, to calculate the Gibbs energy of formation of the homoionic heulandite endmembers without introducing significantly more error than is inherited from experimental determinations of the Gibbs energy of formation.

Estimation of Thermodynamic Properties of Ca^{2+} - Sr^{2+} Exchange in Heulandite

As noted above, slow reaction kinetics of the Ca/Sr ion exchange in heulandite prevented measurement of equilibrium exchange isotherms for the Ca^{2+} - Sr^{2+} binary system. However, the triangle rule allows calculation of the equilibrium constant for the Ca/Sr exchange reaction from the equilibrium constants of either the Ca/Na and Sr/Na exchange reaction or the Ca/K and Sr/K exchange reactions, listed in table 15. The calculated values for $\ln K_{Ca/Sr}$ computed from the Ca/Na and Sr/Na equilibrium constants are equal to 1.87 and 1.94 at 55 and 85 °C, respectively. Comparable values computed using the equilibrium constants for the Ca/K and Sr/K exchange are 2.57 and 2.58 at 55 and 85°C, respectively. Consequently, we can take $\ln K_{Ca/Sr}$ to be equal to 2.25 ± 0.35 apparently independent of temperature.

The Margules parameters for the Ca-Sr binary solid solution in heulandite can be approximated by assuming that the properties of mixing in this binary solid solution in heulandite are identical to those of the Ca/Sr solid solution in the isostructural clinoptilolite. The validity of this approach is supported by the generally good agreement between computed excess Gibbs energies of mixing along the binary solid solutions in

heulandite that are considered in this study (computed using the data in table 15) and the corresponding solid solutions in clinoptilolite (computed using data reported by Pabalan, 1994, and Pabalan and Bertetti, 1999). We used isotherm data for the Ca/Sr exchange in clinoptilolite from Ames (1964) to regress values for $W_{Ca\text{-}Sr}$ and $W_{Sr\text{-}Ca}$ and the resulting values were -1,830 ± 1,140 and 6,610 ± 426 J mol^{-1} K^{-1}.

The curves in figure 13 represent isotherms for Ca/Sr exchange in heulandite computed using the $\ln K_{Ca/Sr}$ determined in this study (2.25). The dashed curve represents ideal solid solution model (that is, Margules parameters equal to zero) and the solid curve was calculated using the Margules parameters regressed from Ames' (1964) experimental data. The unusual shape of the solid isotherm in figure 13 may be a result of combining data from different sources, i.e., using an equilibrium constant derived from the results of this study via the triangle rule on one hand and Margules parameters from Ames' (1964) clinoptilolite data on the other. Inspection of figure 13 shows that the two isotherms differ significantly. The non-ideal model predicts higher selectivity for Sr near the compositional extrema (that is, very high or very low concentrations of Ca) but lower selectivity for Sr at intermediate compositions, compared to the ideal model. The discrepancy between the ideal and non-ideal models is most critical with respect to natural systems at high Ca/Sr ratios of the aqueous solution because Sr is generally in much lower concentrations in natural solutions than Ca. Presently, there is little data available that allows us to conclusively determine the applicability of either of the two solid solution models represented by the two isotherms in figure 13. However, observed concentrations of Ca^{2+} and Sr^{2+} of ground waters in Skagafjördur, northern Iceland, where heulandite is likely present in the aquifers, indirectly support the validity of the

non-ideal solid solution model (Fridriksson and others, in prep.). Ca/Sr ratios of heulandite in equilibrium with the Skagafjördur ground waters calculated using the non-ideal solid solution model for Ca/Sr exchange in heulandite were very close to measured Ca/Sr ratios of natural heulandite from Tertiary basalts in Iceland. Corresponding calculations using the ideal solid solution model predicted Sr concentrations of coexisting heulandite about 10 to 20 times lower than what is observed.

Water Stoichiometry of Heulandite Ion-Exchange Reactions

Thermogravimetric determinations of the water content of fully hydrated Ca-, K-, and Na-heulandite at room temperature (table 1) and experimentally determined thermodynamic properties of hydration/dehydration of Ca-, K-, and Na-clinoptilolite reported by Carey and Bish (1996) allow evaluation of the water stoichiometry of the heulandite ion exchange reactions involving these cations at elevated temperatures. Although the water stoichiometry of the ion-exchange reactions considered in this study does not affect regressed values of ln$K$, $W_{\text{A-B}}$, and $W_{\text{B-A}}$ (c.f., equation 15; because a_{H_2O} of the experimental solutions is taken to be equal to unity), further application of the regressed thermodynamic data, such as for calculation of the relative Gibbs energy difference between the different homoionic endmembers at the experimental temperatures requires explicit consideration of the water stoichiometry of the exchange reactions. The water stoichiometry of the heulandite ion-exchange reactions involving Ca^{2+}, K^{+}, and Na^{+} at 55 and 85 °C, listed in table 15, were approximated through calculations using thermodynamic data for dehydration in Ca-, K-, together with Na-exchanged clinoptilolite (Carey and Bish, 1996) and the water content of the homoionic

heulandite endmembers at room temperature, determined in this study (table 1). In the absence of experimental determination of the thermodynamic properties of hydration/dehydration in homoionic heulandite endmembers we assume that the thermodynamic properties of dehydration for the homoionic clinoptilolite endmembers are identical to the properties of dehydration for the corresponding homoionic heulandite endmembers. The computed dehydration of Ca-heulandite in equilibrium with a liquid saturated water vapor (corresponding to 0.15752 bar P_{H_2O} at 55 ºC and 0.57815 bar P_{H_2O} at 85 ºC; Haar and others, 1984) is equal to 5.1 and 7.9% at 55 and 85 ºC, respectively, relative to water saturation at room temperature. Corresponding values for relative dehydration of K-heulandite are 9.0 and 13.2% at 55 and 85 ºC and 8.7 and 12.0% for Na-heulandite at these temperatures.

The Effect of Temperature on Ion-Exchange Equilibria in Heulandite

Although experimental determinations of equilibrium constants for ion-exchange reactions at two temperatures do not allow accurate retrieval of the standard enthalpies of the reactions, the temperature dependence of the equilibrium constants in table 15 does, nevertheless, provide rough constraints on the heats of these reactions. The relationship between the change of the equilibrium constant as a function of temperature to the enthalpy of the reaction, ΔH°_R, at constant pressure, is described by the van't Hoff equation:

$$\left(\frac{\partial \ln K}{\partial T}\right)_P = \frac{\Delta H^\circ_R}{RT^2}. \qquad (19)$$

It can be seen from table 15 that the equilibrium constants for the Ca/Na, Ca/K, Sr/Na, Sr/K, and K/Na all become more negative with increasing temperature, indicating that these ion-exchange reactions are all exothermic, that is have negative heats of reaction (c.f. equation 19). Assuming, as a first order approximation, that the ion-exchange reactions in table 15 involve no change in heat capacity (that is $\Delta C_P = 0$), and ignoring the continuous dehydration of the mineral as a function of temperature, the heats of these reactions calculated by equation (19) are equal to approximately -12.5 to –14.5 kJ eq^{-1}. Negative heat of the K/Na exchange reaction, associated with incorporation of ~0.5 moles of molecular water into the zeolite, is consistent with negative hydration enthalpies for zeolites, which are typically of the order of –31 kJ per mol of H_2O (c.f. Fridriksson and others, 2003; Bish and Carey, 2001). However, the Ca/Na and Ca/K exchange reactions appear to have negative enthalpies despite the release of 0.4 and 0.85 moles of H_2O per charge equivalent (see table 15).

Heulandite Cation Selectivities

Zeolite cation selectivity sequences describe the relative affinity of a given mineral to incorporate different ions into its crystal structure *via* ion exchange (Colella, 1996). Reported cation selectivity sequences for zeolites show that they will generally prefer larger cations to smaller cations with the same charge (see reviews by Colella, 1996 and Tsitsishvili and others, 1992). This is particularly true for the alkaline earth metal cations while the selectivity sequences for alkali metal cations more often deviate from this pattern. Sherry (1969) explained the observed preference of zeolites for larger ions, with low charge to radius ratio, as a result of relatively low anionic field strength of zeolite

framework. The apparent preference of zeolites for larger cations in exchange equilibrium with an aqueous solution is a result of the strong preference of the aqueous solution for the smaller cations. In other words, the difference in Gibbs energies of hydration between larger and smaller cations with the same charge is more important for the Gibbs energy of an ion exchange reaction than corresponding Gibbs energy differences for the ions in the zeolite crystal structure.

Inspection of table 15 shows that the cation selectivity sequence of heulandite is comparable to other zeolites. For example, the negative values for the ln*K*'s of K/Na exchange reactions in heulandite demonstrate the preference of heulandite for K^+ over Na^+. Similarly, calculated values of ln*K* for Ca/Sr exchange, equal to about 2.25, demonstrates that heulandite prefers Sr^{2+} to Ca^{2+}.

The anionic field strength, or the charge density of the zeolite framework is a function of the framework Si/Al ratio. A necessary consequence of Sherry's (1969) anionic field strength theory is that high-silica low-aluminum zeolites will show stronger preference for larger cations and cations of lower charge compared to low-silica high-aluminum zeolites. As noted above the HEU-framework zeolites, heulandite and clinoptilolite, are isostructural with respect to tetrahedral framework topology but differ by their Si/Al ratios and consequently by their anionic field strengths. It is, therefore, of interest to compare the observed ion-exchange properties of HEU-framework zeolites, heulandite (higher framework charge) and clinoptilolite (lower framework charge) in the context of Sherry's (1969) anionic field strength theory.

Comparison of the equilibrium constants for ion-exchange reactions in heulandite at 55 and 85 °C, determined in this study, to equilibrium constants for corresponding ion-

exchange reactions in clinoptilolite at 25 °C, reported by Pabalan (1994) and Pabalan and Bertetti (1999) shows that these data agree well with Sherry's (1969) anionic field strength theory. For example, the ln*K* for K/Na exchange in clinoptilolite, equal to –3.11 (Pabalan, 1994), is more negative than corresponding ln*K*'s for K/Na exchange in heulandite at 55 and 85 °C, equal to –2.11 and –2.53, illustrating greater preference for K^+ over Na^+ by clinoptilolite than by heulandite. Similarly, the ln*K* for Ca/K exchange in clinoptilolite, equal to 8.5 (Pabalan and Bertetti, 1999), is much more positive than the corresponding values for Ca/K exchange in heulandite, 2.95, and 2.05 (at 55 and 85 °C, respectively), illustrating significantly greater preference of clinoptilolite for K^+ over Ca^{2+} than is exhibited by heulandite. Comparison of the other cation pairs in table 15 gave comparable results.

Exchange Equilibria between Heulandite and Aqueous Solutions in Metamorphic and Geothermal Systems in Iceland

Heulandite is a very common zeolite in basalts that have undergone regional zeolite facies metamorphism (for example, Schmidt, 1990; Neuhoff and others, 2000) and low-temperature hydrothermal alteration (Kristmannsdóttir and Tómasson, 1978; Bargar, 1994). Neuhoff and others (2000) showed that heulandite in Tertiary basalt lavas in eastern Iceland contains up to ten times as much Sr as the host basalts. They noted that the heulandite – stilbite zone in the lava pile coincides with an observed zone of elevated bulk-rock concentrations of Sr in the basalts reported by Wood and others (1976). They suggested, based on this observation, that during regional burial metamorphism of the lava pile Sr was transported by ground water from the upper levels of the lava pile and

sequestered in the heulandite – stilbite zone by heulandite precipitation and ion-exchange. The basalts in eastern Iceland are lithologically homogeneous, well exposed, have been mapped extensively (Walker, 1960, 1963; Neuhoff and others, 1999; Fridriksson and others, 2001), and have active analogs in Icelandic geothermal systems (Kristmannsdóttir and Tómasson, 1978), providing an excellent natural laboratory to investigate this hypothesized regional transport model for Sr^{2+}. As a means of testing the veracity of predicting the effects of ion exchange by heulandite on the mobility of alkali metal and alkaline earth cations, we compare results of the present study to compositional observations in active and fossil systems in Iceland.

The exchange equilibria between heulandite and geothermal solutions were evaluated by comparing the range of compositions of natural heulandite from Icelandic metamorphic and geothermal systems (with respect to Ca and Na) to computed heulandite compositions assuming ion-exchange equilibrium with geothermal solutions of known compositions. Heulandite commonly occurs as a secondary mineral in basalt hosted low-temperature geothermal systems of Iceland where it forms at temperatures between ~70 and ~110 °C (Kristmannsdóttir and Tómasson, 1978). The composition of the natural heulandite used in the present study, listed in table 1, is typical for heulandite in the geothermal systems and the Tertiary zeolite facies basalts of Iceland. Twenty two selected chemical analyses of heulandite from Icelandic geothermal and metamorphic systems are listed in table 2. Ca^{2+} is always the most abundant extraframework cation, constituting on average ~70% of the total extraframework cations. Sodium is generally the second most abundant extraframework cation, constituting on the average 22% of the extraframework cations but K^{+} content is in rare cases comparable to that of Na^{+}. Finally,

Sr^{2+} is generally the fourth most abundant extraframework cation, amounting to ~1% of the total extraframework cation content (see table 2).

The aqueous solutions in low-temperature geothermal systems in Iceland are generally dilute and of meteoric origin (Arnórsson, 1995; Stefánsson and others, 2001). Sodium is in every case the most common cation in these solutions; Na concentration is generally ~10 to 100 times higher than the concentrations of Ca^{2+} and K^{+}. Calcium is generally the second most common cation in geothermal solutions between 70 and 110 °C although K^{+} concentrations are sometimes comparable to Ca^{2+} and even higher in some cases (Stefánsson and others, 2001). Because Ca^{2+} and Na^{+} are the dominant cations in both the heulandite and the aqueous solutions in Icelandic geothermal systems it is justified, as a first order approximation, to use the thermodynamic data for binary Ca/Na ion-exchange, reported in table 15, to evaluate the ion-exchange equilibria between heulandite and aqueous solutions in these systems with respect to Ca^{2+} and Na^{+}.

We considered 24 geothermal solutions over the temperature range between 75 and 93 °C (samples 16, 38, and 44 from Arnórsson and others, 1983; samples 8709, 8742, 8754, 8820, 8833, 8839, 8920, 8941, 8944, and 8945 from Stefánsson and others, 2001; samples 8555, 8710, 8736, 8832, 8834, 8840, 8856, 8939, 8943, 8945, and 9040 from S. Arnórsson unpubl. data). Equilibrium heulandite compositions, in terms of X_{Ca} (defined as $X_{\mathrm{Ca}} = \dfrac{\overline{n}_{\mathrm{Ca}}}{\overline{n}_{\mathrm{Ca}} + \overline{n}_{\mathrm{Na}}}$), were calculated from the fluid composition by nonlinear solution of equation (14) using the thermodynamic data derived from the Na/Ca 85 exchange experiments listed in table 15. Activity coefficients of the aqueous species and free ion concentrations of Ca^{2+} and Na^{+} were computed by EQ3nr (Wolery, 1991). The resulting

values of computed X_{Ca} for heulandite in equilibrium with the geothermal solutions ranged between 0.68 and 0.79 with an average of 0.74. The corresponding values of X_{Ca} calculated from observed compositions of the 22 natural heulandite in table 2 range between 0.70 and 0.88 with an average of 0.75. This is illustrated on figure 16, depicting the relationship between the solution composition (in terms of $a_{Ca^{2+}} / a_{Na^+}^2$) and the composition of a coexisting heulandite (in terms of X_{Ca}) computed by equations (14) and (17a,b) and thermodynamic data regressed from the Ca/Na 85 experiment listed in table 15. The range of the activity ratio $a_{Ca^{2+}} / a_{Na^+}^2$ for the 24 geothermal solutions is indicated on figure 16 by a shaded horizontal box and the solid horizontal line represents the average value. The range of X_{Ca} for the heulandite listed in table 2 is indicated by a vertical shaded box and the average is shown by a vertical solid line. The excellent agreement between observed and computed heulandite compositions with respect to Ca and Na supports the accuracy the thermodynamic data in table 15, at least for Ca/Na exchange, and, by lending credibility to the experimental approach and thermodynamic model for ion-exchange used in this study, suggests that the remaining data in table 15 can be used to accurately predict the partitioning of Ca^{2+}, Na^+, K^+, and Sr^{2+} between heulandite and coexisting aqueous solutions, at least for binary systems.

ACKNOWLEDGEMENTS

We are grateful to H. Hjörleifsson at Teigarhorn, Iceland for contributing the natural heulandite sample for this study. T. Blöndal, T. Bawden, K. Lemke, K. Savage, and A. Spieler helped with sample preparation and ion-exchange experiments at Stanford University. Help from R. Jones with electron microprobe analyses and scanning electron

microscopy work is greatly appreciated. We are grateful to J. Stebbins at Stanford and J. Bischoff at USGS for allowing use of their laboratories. Logistical help from R. Pletcher at Lawrence Livermore National Laboratory at the initial stages of this study was invaluable. D. Bish at Los Alamos National Laboratory helped with TGA and XRD analyses of homoionic heulandites. G. Li at Stanford University conducted ICP analyses of experimental solutions and solids. S. Arnórsson is gratefully acknowledged for allowing use of his unpublished geothermal fluid analyses. R. Pabalan and J. Mazlan are acknowledged for thoughtful reviews. This research was funded by a grant from the National Science Foundation (NSF EAR 0001113) to D.K. Bird, and by grants from the Shell and McGee Funds at Stanford University, Fulbright, and the American Scandinavian Foundation to Th. Fridriksson.

REFERENCES

Alietti, A., Brigatti, M.F., and Poppi, L., 1977, Natural, Ca-rich clinoptilolites (heulandites of group 3): new data and review: Neues Jahrbuch für Mineralogie, Monatshefte, v. 11, p. 493-501.

Ames, L.L. Jr., 1964, Some zeolite equilibria with alkali metal cations: American Mineralogist, v. 49, p. 127-145.

Anderson, G.M., and Crerar, D.A., 1993, Thermodynamics in Geochemistry: The Equilibrium Model: Oxford University Press, New York, 588 p.

Argersinger, W.J., Davidson, A.W. and Bonner, O.D., 1950, Thermodynamics and Ion Exchange Phenomena: Transactions of the Kansas Academy of Science, v. 53, p. 404-410.

Armbruster, T., 1993, Dehydration mechanism of clinoptilolite and heulandite: Single crystal study of Na-poor, Ca-, K-, Mg-rich clinoptilolite at 100 K: American Mineralogist, v. 78, p. 260-264.

Armbruster, T. and Gunter, M.E., 2001, Crystal structures of natural zeolites, *in* Bish, D.L., and Ming, D.W., editors, Natural Zeolites: Occurrence, Properties, Applications: Mineralogical Society of America Reviews in Mineralogy and Geochemistry, v. 45, p. 1-68.

Arnórsson S., 1995, Geothermal systems in Iceland: Structure and conceptual models – II. Low-temperature areas: Geothermics, v. 24, p. 603-629.

Arnórsson S., Gunnlaugsson H., and Svavarsson H., 1983, The chemistry of geothermal waters in Iceland II. Mineral equilibria and independent variables controlling water compositions: Geochimica et Cosmochimica Acta, v. 47, p. 547-566.

Bargar K. E., 1994, Hydrothermal alteration in the SUNEDCO 58-28 geothermal drill hole near Breitenbush Hot Springs, Oregon: Oregon Geology, v. 56, p. 75-87.

Benning, L.G., Wilkin, R.T., and Barnes, H.L., 2000, Solubility and stability of zeolites in aqueous solution: II. Calcic clinoptilolite and mordenite: American Mineralogist, v. 85, p. 495-508.

Bish, D.L. and Carey, J.W., 2000, Coupled X-ray powder diffraction and thermogravimetric analysis of clinoptilolite dehydration behavior, *in* Colella, C., and Mumpton, F. A., editors: Natural Zeolite for the Third Milennium: Naples, Italy, De Frede Editore, p. 249-257.

Bish, D.L. and Boak J.M. (2001) Clinoptilolite-Heulandite Nomenclature, *in* Bish, D.L., and Ming, D.W., editors, Natural Zeolites: Occurrence, Properties, Applications: Mineralogical Society of America Reviews in Mineralogy and Geochemistry, v. 45, p. 207-216.

Bish, D.L. and Carey, J.W. (2001) Thermal Properties of Natural Zeolites, *in* Bish, D.L., and Ming, D.W., editors, Natural Zeolites: Occurrence, Properties, Applications: Mineralogical Society of America Reviews in Mineralogy and Geochemistry, v. 45, p. 403-452.

Broxton, D.E., Bish, D.L., and Warren, R.G., 1987, Distribution and chemistry of diagenetic minerals at Yucca Mountain, Nye County, Nevada: Clays and Clay Minerals, v. 35, p. 89-110.

Carey, J.W. and Bish, D.L., 1996, Equilibrium in the clinoptilolite-H_2O system: American Mineralogist, v. 81, 952-962.

Carey, J.W. and Bish, D.L., 1997, Calorimetric measurement of the enthalpy of hydration of clinoptilolite: Clays and Clay Minerals, v. 45, 826-833.

Colella, C., 1996, Ion exchange equilibria in zeolite minerals: Mineral Deposita v. 31, p. 552-562.

Coombs, D. S., Alberti, A., Armbruster, T., Artioli, G., Colella, C., Galli, E., Grice, J. D., Liebau, F., Mandarino, J. A., Minato, H., Nickel, E. H., Passaglia, E., Peacor, D. R., Quartieri, S., Rinaldi, R., Ross, M., Sheppard, R.A., Tillmanns, E., and Vezzalini, G., 1998, Recommended nomenclature for zeolite minerals: Report of the subcommittee on zeolites of the International Mineralogical Association, Commission on New Minerals and Mineral Names: Mineralogical Magazine, v. 62, p. 1571-1606.

Fridriksson, Th., Neuhoff, P.S., Arnórsson, S., and Bird, D.K., 2001, Geological constraints on the thermodynamic properties of the stilbite-stellerite solid solution in low-grade metabasalts: Geochimica et Cosmochimica Acta, v. 65, p. 3993-4008.

Fridriksson, Th., Carey, J.W., Bish, D.L., Neuhoff, P.S., and Bird, D.K., 2003, Hydrogen-bonded water in laumontite II: Experimenal determination of site-specific

thermodynamic properties of hydration of the W1 and W5 sites: American Mineralogist, v. 88, p. 1060-1072.

Fridriksson, Th., Arnórsson, S., and Bird, D.K., in preparation, Processes controlling Sr concentrations in natural waters in Skagafjordur, a Tertiary tholeiitic floodbasalt provence in northern Iceland: In preparation for Geochimica et Cosmochimica Acta.

Gaines, G.L. and Thomas, H.C., 1953, Adsorption studies on Clay Minerals II. Formulation of the Thermodynamics of Exchange Adsorption: The Journal of Chemical Physics, v. 21, p. 89-113.

Gottardi, G. and Galli, E., 1985, Natural Zeolites: Berlin Heidelberg, Springer-Verlag, 407 p.

Haar, L., Gallagher, J.S., and Kell, G.S., 1984, NBS/NRC Steam Tables: Thermodynamic and Transport Properties and Computer Programs for Vapor and Liquid Sates of Water in SI Unites: Washington D.C., Hemisphere Publishing, 320 p.

Illman, D.L., 1993, Researchers take up environmental challenge at Hanford, Stark pollution problems at former nuclear production site call forth unprecedented technological effort that may stretch out for decades: Chemical & Engineering News, June 21, p 9-21.

Johnson, G.K., Flotow, H.E., Ohare, P.A.G., and Wise, W.S., 1985, Thermodynamic studies of zeolites: Heulandite: American Mineralogist, v. 70, p. 1065-1071.

Johnson, G.K., Tasker, I.R., Jurgens, R., and Ohare, P.A.G., 1991, Thermodynamic studies of zeolites: clinoptilolite: Journal of Chemical Thermodynamics, v. 23, 475-484.

Johnson, J.W., Oelkers, E.H., and Helgeson, H.C., 1992, SUPCRT92: Software package for calculating the standard molar thermodynamic properties of minerals, gases, aqueous species, and reactions among them as functions of temperature and pressure: Computers in Geoscience, v. 18, p. 899-947.

Kalló, D., 2001, Applications of Natural Zeolites in Water and Wastewater Treatment, *in* Bish, D.L., and Ming, D.W., editors, Natural Zeolites: Occurrence, Properties, Applications: Mineralogical Society of America Reviews in Mineralogy and Geochemistry, v. 45, p. 519-550.

Kato, M., Satokawa, S., and Itabashi, K., 1997, Synthetic clinoptilolite and distribution of aluminum atoms in the framework of HEU type zeolites, *in* Chon, H., Ihm, S.-K., and Uh, Y.S., editors, Progress in Zeolite and Microporous Materials: Studies in Surface Science and Catalysis, v. 105, p. 229-235.

Kiseleva, I., Navrotsky, A., Belitsky, I., and Fursenko, B., 2001, Thermochemical study of calcium zeolites: heulandite and stilbite: American Mineralogist, v. 86, p. 448-455.

Kristmannsdóttir H. and Tómasson J., 1978, Zeolite zones in geothermal areas in Iceland, *in* Sand, L. B., and Mumpton, F. A., editors, Natural Zeolites: Oxford, Pergamon Press Ltd, p. 227-284.

Ming, D.W. and Allen, E.R., 2001, Use of Natural Zeolites in Agronomy, Horticulture, and Environmental soil remediation, *in* Bish, D.L., and Ming, D.W., editors, Natural Zeolites: Occurrence, Properties, Applications: Mineralogical Society of America Reviews in Mineralogy and Geochemistry, v. 45, p. 619-654.

Neuhoff P.S., Fridriksson Th., Arnórsson S., and Bird D.K., 1999, Porosity evolution and mineral paragenesis during low-grade metamorphism of basaltic lavas at Teigarhorn, eastern Iceland: American Journal of Science, v. 299, p. 467-501.

Neuhoff P.S., Fridriksson Th., and Bird D.K., 2000, Zeolite parageneses in the north Atlantic igneous province: Implications for geotectonics and groundwater quality of basaltic crust: International Geology Review, v. 42, p. 15-44.

Nordstrom, D.K. and Munoz, J.L., 1994, Geochemical Thermodynamics: Boston, Blackwell Scientific Publications, 477 p.

Pabalan, R.T., 1991, Nonideality effects on the ion exchange behavior of the zeolite mineral clinoptilolite: Material Research Society Symposium Proceedings, v. 212, p. 559-567.

Pabalan, R.T., 1994, Thermodynamics of ion exchange between clinoptilolite and aqueous solutions of Na^+/K^+ and Na^+/Ca^+: Geochimica et Cosmochimica Acta, v. 58, p. 4573-4590.

Pabalan, R.T., and Bertetti, F.P., 1999, Experimental and Modeling Study of Ion Exchange Between Aqueous Solutions and the Zeolite Mineral Clinoptilolite: Journal of Solution Chemistry, v. 28, p. 367-393.

Pabalan, R.T., and Bertetti, F.P., 2001, Cation-Exchange Properties of Natural Zeolites, *in* Bish, D.L., and Ming, D.W., editors, Natural Zeolites: Occurrence, Properties, Applications: Mineralogical Society of America Reviews in Mineralogy and Geochemistry, v. 45, p. 453-518.

Palmer, J.L. and Gunter, M.E., 2001, The effects of time, temperature, and concentration on Sr^{2+} exchange in clinoptilolite in aqueous solutions: American Mineralogist, v. 86., p.431-437.

Passaglia, E., 1970, The crystal chemistry of chabazites: American Mineralogist, v. 55., p. 1278-1301.

Passaglia, E. and Sheppard, R.A., 2001, Crystal Chemistry of Zeolites, *in* Bish, D.L., and Ming, D.W., editors, Natural Zeolites: Occurrence, Properties, Applications: Mineralogical Society of America Reviews in Mineralogy and Geochemistry, v. 45, p. 69-116.

Saxena, S.K., 1973, Thermodynamics of Rock-Forming Crystalline Solutions: Berlin, Springer-Verlag, 188 p.

Schmidt S. Th., 1990, Alteration under conditions of burial metamorphism in the North Shore Volcanic Group, Minnesota - Mineralogical and geochemical zonation: Heidelberg, Heidelberger Geowissenschaftliche Abhandlungen, 309 p.

Sherry, H.S., 1969, The ion-exchange properties of zeolites, *in* Marinski, J.A., and Dekker, M., editors, Ion exchange: New York, Marcel Dekker, p. 89-133.

Shibue, Y., 1981, Cation-Exchange Reactions of Siliceous and Aluminous Phillipsites: Clays and Clay Minerals, v. 2, p. 397-402.

Shibue, Y., 1998, Cation-exchange properties of phillipsite (natural zeolite): The difference between Si-rich and Si-poor phillipsites: Separation Science and Technology, v. 33, p. 333-335.

Smyth, J.R., Spaid, A.T., and Bish, D.L., 1990, Crystal structures of a natural and a Cs-exchanged clinoptilolite: American Mineralogist, v. 75, 522-528.

Stefánsson A., Gíslason S.R., and Arnórsson S., 2001, Dissolution of primary minerals in natural waters: Chemical Geology, v. 172, p. 251-276.

Sturchio, N.C., Bohlke, J.K., and Binz, C.M., 1989, Radium-thorium disequilibrium and zeolite-water ion exchange in a Yellowstone hydrothermal environment: Geochimica et Cosmochimica Acta, v. 53, p. 1025-1034.

Sturchio, N.C., Bohlke, J.K., and Markun, F.J., 1993, Radium Isotope Geochemistry of Thermal Waters, Yellowstone-National-Park, Wyoming, USA: Geochimica et Cosmochimica Acta , v. 57, p. 1203-1214.

Tsitsishvili, G.V., 1988, Perspectives of natural zeolite application, *in* Kalló, D., and Sherry, H.S., editors, Occurrence, Properties and Utilization of Natural Zeolites: Budapest, Akadémiai Kiadó, p. 367-394.

Tsitsishvili, G.V., Andronikashvili, T.G., Kirov, G.N., and Filizova, L.D., 1992, Natural Zeolites: London, Ellis Horwood, 295 p.

Valcke, E., Engels, B., and Cremers, A., 1997a, The use of zeolites as amendments in radiocaecium- and radiostrontium-contaminated soils: A soil-chemical approach. Part I: Cs-K exchange in clinoptilolite and mordenite: Zeolites, v. 18, p. 205-211.

Valcke, E., Engels, B., and Cremers, A., 1997b, The use of zeolites as amendments in radiocaecium- and radiostrontium-contaminated soils: A soil-chemical approach. Part II: Sr-Ca exchange in clinoptilolite, mordenite, and zeolite A: Zeolites, v. 18, p. 212-217.

Vanselow, A.P., 1932, Equilibria of the base-exchange reactions of bentonites, permutite, soil colloids, and zeolite: Soil Science, v. 33, p. 95-113.

Viani, B.E. and Bruton, C.J., 1992, Modeling of ion exchange in clinoptilolite using EQ3/6 geochemical modeling code, *in* Kharaka, Y.K., and Maest, A.S., editors, Proceedings of the 7th International Symposium on Water-Rock Interaction: Rotterdam, The Netherlands, Balkema, p 73-77.

Walker G. P. L., 1960, Zeolite zones and dike distribution in relation to the structure of the basalts of eastern Iceland: Journal of Geology, v. 68, p. 515-528.

Walker G. P. L., 1963, The Breiddalur central volcano, eastern Iceland [with discussion], Quarterly Journal of the Geological Society of London, v. 119, p. 26-63.

Ward, R.L., and McKague, H.L., 1994, Clinoptilolite and heulandite structural differences as revealed by multinuclear nuclear magnetic resonance spectroscopy: Journal of Physical Chemistry, v. 98, p. 1232-1237.

White, A.F., Claasen, H.C., and Benson, L.V., 1980, The effect of glass dissolution on the water chemistry in a tuffaceous aquifer, Ranier Mesa, Nevada: U.S.G.S. Water Supply Paper 1535-Q, 30 p.

White, D.A., Nattkemper, A., and Rautiu, R., 1999, Evaluation of the effects of temperature on potassium clinoptiolite ion exchange: Nuclear Technology, v. 127, p. 212-217.

Wilkin, R.T. and Barnes, H.L., 1998, Solubility and stability of zeolites in aqueous solution: I. Analcime, Na-, and K-clinoptilolite, American Mineralogist: v. 83, p. 746-761.

Wilkin, R.T. and Barnes, H.L., 1999, Thermodynamics of hydration of Na- and K-clinoptilolite to 300 °C: Physics and Chemistry of Minerals, v. 26, 468-476.

Wolery, T.J., 1991, EQ3nr. A computer program for geochemical aqueous speciation solubility calculations: Theoretical manual, user's guide and related documentation (Version 7.0): Lawrence Livermore National Laboratory.

Wood, D.A., Gibson, I.L., and Thompson, R.N., 1976, Elemental mobility during zeolite facies metamorphism of the Tertiary basalts of eastern Iceland: Contributions to Mineralogy and Petrology, v. 55, p. 241-254.

Woods, R.M. and Gunter, M.E., 2001, Na- and Cs-exchange in a clinoptilolite-rich rock: Analysis of the outgoing cations in solution: American Mineralogist, v. 86, p. 424-430.

Yang, S.Y., Navrotsky, A., and Wilkin, R., 2001, Thermodynamics of ion-exchanged and natural clinoptilolite: American Mineralogist, v. 86, p. 438-447.

Figure captions

Figure 1. Compositions of selected HEU-framework minerals (heulandite and clinoptilolite) in terms of fraction of divalent cations as a function of aluminum content. The bulk composition of the heulandite powder used in the present study is shown by a large solid circle. Electron microprobe analyses of selected crystal fragments of the heulandite used in this study are shown by smaller solid symbols. See legend for sources of other data.

Figure 2. SEM images of untreated and ion-exchanged heulandite. The untreated heulandite (A) has very sharp edges. A few small (<1 μm) crystal fragments are visible in the upper corner of the grain and near the right edge of the image. The ion-exchanged heulandite (B) from the Na/Sr 85-23 experiment exhibits some rounding of edges that is likely due to dissolution. Note that submicron crystal fragments are still present on the surface of the grain after a total of 11 weeks of ion-exchange at 85 to 90 ºC.

Figure 3. Results of the Ca/Na 55 (squares) and Na/Ca 55 (circles) ion-exchange experiments shown in terms of equivalent fraction of Ca in the heulandite as a function of the equivalent fraction of Ca in the aqueous solution. The larger, solid symbols represent data where the solid phase composition was determined by ICP-AES. The smaller, shaded symbols represent data where the solid phase composition was computed from the fluid analyses. The open symbols represent the computed solid phase compositions for samples that were analyzed by ICP-AES. Data represented by the open symbols were

omitted from thermodynamic analysis. The solid curve represents an equilibrium ion-exchange isotherm computed from regressed thermodynamic data for the Ca/Na ion-exchange reaction at 55 ºC listed in table 15.

Figure 4. Results of the K/Ca 55 ion-exchange experiments shown in terms of equivalent fraction of Ca in the heulandite as a function of the equivalent fraction of Ca in the aqueous solution. See figure caption to figure 3 for explanation of symbols and curves.

Figure 5. Results of the K/Na 55 ion-exchange experiments shown in terms of equivalent fraction of K in the heulandite as a function of the equivalent fraction of K in the aqueous solution. See figure caption to figure 3 for explanation of symbols and curves.

Figure 6. Results of the K/Sr 55 ion-exchange experiments shown in terms of equivalent fraction of Sr in the heulandite as a function of the equivalent fraction of Sr in the aqueous solution. See figure caption to figure 3 for explanation of symbols and curves.

Figure 7. Results of the Na/Sr 55 ion-exchange experiments shown in terms of equivalent fraction of Sr in the heulandite as a function of the equivalent fraction of Sr in the aqueous solution. See figure caption to figure 3 for explanation of symbols and curves.

Figure 8. Results of the Ca/K 85 (squares) and K/Ca 85 (circles) ion-exchange experiments shown in terms of equivalent fraction of Ca in the heulandite as a function of the equivalent fraction of Ca in the aqueous solution. See figure caption to figure 3 for explanation of symbols and curves.

Figure 9. Results of the K/Sr 85 ion-exchange experiments shown in terms of equivalent fraction of Sr in the heulandite as a function of the equivalent fraction of Sr in the aqueous solution. See figure caption to figure 3 for explanation of symbols and curves.

Figure 10. Results of the Na/Ca 85 ion-exchange experiments shown in terms of equivalent fraction of Ca in the heulandite as a function of the equivalent fraction of Ca in the aqueous solution. See figure caption to figure 3 for explanation of symbols and curves.

Figure 11. Results of the Na/K 85 ion-exchange experiments shown in terms of equivalent fraction of K in the heulandite as a function of the equivalent fraction of K in the aqueous solution. See figure caption to figure 3 for explanation of symbols and curves.

Figure 12. Results of the Na/Sr 85 ion-exchange experiments shown in terms of equivalent fraction of Sr in the heulandite as a function of the equivalent fraction of Sr in

the aqueous solution. See figure caption to figure 3 for explanation of symbols and curves.

Figure 13. Results of the Ca/Sr 55 (circles) and Ca/Sr 85 (squares) ion-exchange experiments shown in terms of equivalent fraction of Ca in the heulandite as a function of the equivalent fraction of Ca in the aqueous solution. All solid compositions were computed from the fluid analyses. The curves represent ion-exchange isotherms computed using an equilibrium constant determined from the exchange reactions in table 15 via the triangle rule. The dashed curve represents an ion exchange isotherm computed assuming ideal behavior of the Ca/Sr solid solution and the solid curve represents an isotherm computed using Margules parameters regressed from Ca/Sr exchange data from Ames (1964).

Figure 14. Results of the Ca/Na 55 (squares) and Na/Ca 55 (circles) ion-exchange experiments shown in terms $\ln k_{V(Ca/Na)}$ as a function of the mole fraction of Ca in the solid phase. The larger, solid symbols represent data where the solid phase composition was determined by ICP-AES. The smaller, shaded symbols represent data where the solid phase composition was computed from the fluid analyses. The solid curve was calculated using the equilibrium constant and the Margules parameters that were regressed from this data set.

Figure 15. Results of the Na/Ca 85 ion-exchange experiments shown in terms $\ln k_{V(Ca/Na)}$ as a function of the mole fraction of Ca in the solid phase. See caption to figure 14 for explanation of symbols.

Figure 16. Comparison of predicted and observed heulandite compositions in geothermal and metamorphic systems in Iceland. The solid curve represents the relationship between the compositions of aqueous solutions (in terms of $\ln a_{Ca^{2+}} - 2\ln a_{Na^{+}}$) and coexisting heulandite (in terms of X_{Ca}) computed from the thermodynamic data in table 15 (Na/Ca85). The shaded horizontal box shows the range of $a_{Ca^{2+}} / a^2_{Na^{+}}$ observed in 24 geothermal solutions from Iceland and the average value is indicated by the solid horizontal line. The shaded vertical box depicts the range of observed heulandite compositions (table 2) and the average is indicated by the solid vertical line.

Table 1. Compositions of natural and homoionic heulandites

	natural heulandite	Na-heulandite	Ca-heulandite	K-heulandite
Si[a,b]	6.78	6.78	6.75	6.75
Ti[a,b]	0.01	0.01	0.01	n.d.
Fe[a,b]	0.04	0.05	0.03	0.00
Cr[a,b]	0.00	0.00	0.00	0.00
Al[a,b]	2.17	2.18	2.18	2.17
Mg[a,b]	0.01	0.02	0.01	0.00
Mn[a,b]	0.00	0.00	0.00	n.d.
Ca[a,b]	0.90	0.02	1.04	0.01
Ba[a,c]	0.01	0.01	0.01	0.01
Sr[a,c]	0.03	0.01	0.02	0.00
Na[a,b]	0.26	2.05	0.06	0.01
K[a,b]	0.05	0.00	0.02	2.05
H_2O[a,d]		6.48	7.13	5.41
E%[e]	1.84	-0.46	2.75	-3.23
CEC[f] (meq/g)		2.97	2.90	2.92

[a] atoms per 18 framework oxygen atoms. [b] determined by ICP AES. [c] determined by ICP MS. [d] determined by TGA. [e] charge balance error (see Passaglia, 1970). [f] see equation (4) for definition of CEC.

Table 2. Selected heulandite analyses from Icelandic geothermal and metamorphic systems

Sample id	ISXRF2B	ISXRF2 [b]	ISXRF4[c]	ISXRF5[d]	ISXRF6[c]	ISXRF7[d]	ISXRF8[b]	ISXRF9[e]	LJ 8 76m[f]	LJ 8 150m[f]	LJ 8 370m[f]
analytical	XRF	EMPA	XRF	XRF	XRF	XRF	XRF	XRF	EMPA	EMPA	EMPA
Si[a]	6.77	6.73	6.79	6.77	6.74	6.80	6.82	6.78	6.93	7.07	6.91
Al[a]	2.23	2.30	2.21	2.24	2.27	2.25	2.18	2.21	2.10	1.97	2.14
Mg[a]	0.00	0.00	0.01	0.00	0.00	0.01	0.00	0.00	0.00	0.00	0.00
Ca[a]	0.91	0.89	0.90	0.89	0.91	0.76	0.91	0.92	0.81	0.80	0.90
Na[a]	0.33	0.36	0.32	0.36	0.37	0.29	0.31	0.28	0.32	0.19	0.12
K[a]	0.05	0.05	0.05	0.04	0.04	0.24	0.05	0.04	0.05	0.04	0.05
Sr[a]	0.04	0.00	0.03	0.04	0.04	0.07	0.04	0.04	na	na	na

Table 2 cont'd. Selected heulandite analyses from Icelandic geothermal and metamorphic systems

Sample id	H 1[d]	H 2[g]	H 3[h]	H 4[i]	H 5[c]	H 8[e]	NÍ 14692[j]	NÍ 1582[k]	NÍ 14320[l]	HIX 11[m]	HIX 5[m]
analytical	ICP	ICP	ICP	ICP	ICP	ICP	ICP	ICP	ICP	EMPA	EMPA
Si[a]	6.88	6.77	6.88	6.88	6.86	6.91	6.80	6.80	6.75	6.90	6.74
Al[a]	2.11	2.19	2.11	2.10	2.12	2.07	2.15	2.08	2.18	2.11	2.28
Mg[a]	0.02	0.01	0.01	0.01	0.01	0.01	0.00	0.01	0.02	0.00	0.00
Ca[a]	0.82	0.95	0.84	0.87	0.90	0.87	0.87	0.99	0.86	0.88	0.92
Na[a]	0.18	0.26	0.27	0.27	0.26	0.26	0.36	0.34	0.35	0.27	0.24
K[a]	0.16	0.06	0.05	0.07	0.05	0.06	0.07	0.06	0.11	0.06	0.12
Sr[a]	0.02	0.02	0.02	0.02	0.01	0.01	0.02	0.02	0.05	na	na

[a] atoms per 18 framework oxygen atoms. [b] hydrothermal; upper Berufjördur valley, eastern Iceland. [c] hydrothermal; Tinnudalur in Breiddalur, eastern Iceland. [d] hydrothermal; Breiddalur, eastern Iceland. [d] hydrothermal; Djúpivogur, eastern Iceland. [e] metamorphic; Teigarhorn, Berufjördur,eastern Iceland. [f] hydrothermal; drill cuttings, hole LJ8 Laugaland, Eyjafjördur, northern Iceland. [g] metamorphic; Fossárdalur, Berufjördur, eastern Iceland. [h] hydrothermal; Búlandsá, Berufjördur, eastern Iceland. [i] metmorphic; Berunes, Berufjördur, eastern Iceland. [j] metamorphic; Oddsskard, eastern Iceland. [k] metamorphic; Berufjördur, eastern Iceland. [l] metamorphic; Hvalfjördur, southwest Iceland. [m] hydrothermal; Teigarhorn, Berufjördur,eastern Iceland.

Table 3. Experimental details and results of Ca/Na exchange experiments at 55 °C[a]

sample id	Ca-heulandite (mg)	Ca-stock [b] (g of solution)	Na-stock [c] (g of solution)	weight loss (g)	$m\mathrm{Ca}^{2+}$ [d] mmol/kg	$m\mathrm{Na}^{+}$ [d] mmol/kg	X_{Ca} [e] calculated	X_{Ca} ICP
Ca/Na 55-1	59	14.998	0.058	0.595	52.192	0.264	0.977	
Ca/Na 55-2	52	15.448	0.017	0.592	52.090	0.090	0.995	
Ca/Na 55-3	51.5	15.143	0.03	0.613	52.183	0.165	0.992	
Ca/Na 55-4	50.5	14.967	0.115	0.623	52.128	0.557	0.953	
Ca/Na 55-5	61	14.935	0.074	0.617	51.197	0.323	0.970	
Ca/Na 55-6	51	14.969	0.12	0.601	51.283	0.595	0.956	
Ca/Na 55-7	48	14.854	0.158	0.596	50.634	0.814	0.946	
Ca/Na 55-8	57	14.736	0.294	0.61	50.947	1.594	*0.927* [f]	0.918
Ca/Na 55-9	55	15.085	0.446	0.624	50.461	2.507	0.916	
Ca/Na 55-10	49	14.45	0.8	0.612	49.373	4.971	0.906	
Ca/Na 55-11	53	13.433	1.501	0.625	47.282	9.773	0.873	
Ca/Na 55-12	55	12.504	2.349	0.606	44.663	15.637	0.839	
Ca/Na 55-13	50	11.638	3.278	0.61	41.712	22.343	0.834	
Ca/Na 55-14	57	9.642	5.48	0.585	34.536	36.910	0.766	
Ca/Na 55-15	53	8.52	6.417	0.574	31.070	44.272	*0.761* [f]	0.754
Ca/Na 55-16	66	7.435	7.385	0.621	27.737	50.701	0.718	
Ca/Na 55-17	54	6.517	8.577	0.623	24.092	58.460	0.671	
Ca/Na 55-18	54	4.481	10.305	0.647	17.368	71.111	0.613	
Ca/Na 55-19	25	7.572	42.07	0.58	7.938	85.440	0.536	
Ca/Na 55-20	18	3.777	45.91	0.61	4.041	92.823	0.429	
Ca/Na 55-21	19	0	49.987	0.61	0.348	99.646	0.230	
Ca/Na 55-22	13	0	50.242	0.63	0.274	101.08	0.167	
Ca/Na 55-23	11	0	50.078	0.60	0.219	100.55	0.192	
Ca/Na 55-24	5.5	0	50.888	0.61	0.127	99.923	0.109	

[a] 96 days in oven, [b] concentration = 0.0496 mol/kg, [c] concentration = 0.0994 mol/kg, [d] uncorrected ICP data, [e] calculated from weight corrected aqueous cation concentrations according to equations (1), (3), and (5).

Table 4. Experimental details and results of Na/Ca exchange experiments at 55 °C[a]

sample id	Na-heulandite (mg)	Ca-stock [b] (g of solution)	Na-stock [c] (g of solution)	weight loss (g)	$m\mathrm{Ca}^{2+}$ [d] mmol/kg	$m\mathrm{Na}^{+}$ [d] mmol/kg	X_{Ca} [e] calculated	X_{Ca} ICP
Na/Ca 55-1	51	0.055	14.957	0.849	0.037	105.72	0.015	
Na/Ca 55-2	52	0.056	30.515	0.856	0.018	102.44	0.015	
Na/Ca 55-3	52	0.08	14.968	0.843	0.041	105.30	0.023	
Na/Ca 55-4	48	0.115	14.863	0.864	0.046	104.38	0.037	
Na/Ca 55-5	55	0.3065	14.744	0.809	0.115	103.31	0.092	
Na/Ca 55-6	64	0.451	14.545	0.83	0.151	103.00	0.121	
Na/Ca 55-7	54	0.653	14.593	0.815	0.376	100.77	0.204	
Na/Ca 55-8	47	1.06	13.909	0.885	1.329	103.30	*0.327* [f]	0.389
Na/Ca 55-9	54	1.544	13.57	0.836	2.196	99.889	0.398	
Na/Ca 55-10	47	2.644	12.566	0.93	6.053	93.443	0.478	
Na/Ca 55-11	50	4.911	10.206	0.933	13.780	80.039	0.540	
Na/Ca 55-12	63	6.612	8.64	0.924	18.453	70.897	0.594	
Na/Ca 55-13	65	8.468	6.994	0.939	24.262	59.584	*0.658* [f]	0.686
Na/Ca 55-14	52	11.087	3.911	0.938	35.541	37.738	0.721	
Na/Ca 55-15	51	11.842	3.112	0.917	38.111	31.861	0.752	
Na/Ca 55-16	61	12.751	2.369	0.927	39.821	28.064	0.772	
Na/Ca 55-17	52	13.409	1.679	0.915	42.505	21.519	0.803	
Na/Ca 55-18	65	23.588	0.906	0.936	46.296	11.184	0.824	
Na/Ca 55-19	25	48.252	1.604	0.93	49.156	4.759	0.891	
Na/Ca 55-20	22	49.475	0.577	0.95	50.555	2.465	0.895	
Na/Ca 55-21	20	49.695	0	0.93	51.297	1.173	0.909	
Na/Ca 55-22	15	49.787	0	0.93	51.684	0.845	0.840	
Na/Ca 55-23	9	49.54	0	0.94	51.717	0.511	0.846	
Na/Ca 55-24	4	52.227	0	0.93	52.117	0.230	0.954	

[a] 135 days in oven, [b] concentration = 0.0496 mol/kg, [c] concentration = 0.0994 mol/kg, [d] uncorrected ICP data, [e] calculated from weight corrected aqueous cation concentrations according to equations (1), (3), and (5).

Table 5. Experimental details and results of K/Ca exchange experiments at 55 °C[a]

sample id	K-heulandite (mg)	Ca-stock [b] (g of solution)	K-stock [c] (g of solution)	weight loss (g)	$m\mathrm{Ca}^{2+}$ [d] mmol/kg	$m\mathrm{K}^{+}$ [d] mmol/kg	X_{Ca} [e] calculated	X_{Ca} ICP
K/Ca 55-1	76	0.037	21.917	0.425	0.037	101.41	0.005	
K/Ca 55-2	70	0.066	21.998	0.389	0.075	100.47	*0.008* [f]	0.009
K/Ca 55-3	58	0.095	22.198	0.412	0.123	100.00	0.012	
K/Ca 55-5	52	0.441	21.749	0.426	0.779	98.441	0.033	
K/Ca 55-6	85	0.607	21.269	0.408	0.993	97.871	0.036	
K/Ca 55-7	73	0.855	21.228	0.396	1.540	98.301	*0.046* [f]	0.052
K/Ca 55-8	68	1.392	20.831	0.398	2.676	96.115	0.059	
K/Ca 55-9	54	2.008	20.000	0.378	4.235	95.166	0.072	
K/Ca 55-10	58	3.633	18.297	0.354	7.783	87.972	*0.112* [f]	0.114
K/Ca 55-11	65	6.452	15.594	0.376	14.432	76.934	0.133	
K/Ca 55-12	69	8.827	13.479	0.364	19.304	66.464	0.189	
K/Ca 55-13	72	11.383	11.079	0.367	24.947	56.247	0.248	
K/Ca 55-14	70	14.914	7.342	0.405	32.664	39.648	0.356	
K/Ca 55-15	58	15.706	6.327	0.431	35.525	34.842	0.379	
K/Ca 55-16	63	17.1175	5.017	0.385	37.797	29.003	0.443	
K/Ca 55-17	64	17.733	4.386	0.546	39.052	26.394	0.478	
K/Ca 55-18	56	19.28	2.625	0.559	43.062	18.030	0.560	
K/Ca 55-20	19	48.753	1.064	0.66	49.392	3.237	0.881	
K/Ca 55-21	17	49.924	0	0.65	50.742	0.971	0.914	
K/Ca 55-22	17	51.1125	0	0.73	50.519	0.923	0.877	
K/Ca 55-23	11	52.03	0	0.66	50.265	0.621	0.994	
K/Ca 55-24	7	51.44	0	0.69	50.870	0.353	0.775	

[a] 72 days in oven, [b] concentration = 0.0498 mol/kg, [c] concentration = 0.0995 mol/kg, [d] uncorrected ICP data, [e] calculated from weight corrected aqueous cation concentrations according to equations (1), (3), and (5). [f] value not used in thermodynamic analyses.

Table 6. Experimental details and results of K/Na exchange experiments at 55 °C[a]

sample id	K-heulandite (mg)	K-stock [b] (g of solution)	Na-stock [c] (g of solution)	weight loss (g)	$m\mathrm{K}^{+}$ [d] mmol/kg	$m\mathrm{Na}^{+}$ [d] mmol/kg	X_{K} [e] calculated	X_{K} ICP
K/Na 55-1	57	22.231	0.038	0.377	102.38	0.189	*1.002* [f]	
K/Na 55-2	71	22.182	0.023	0.386	106.27	0.138	*1.003* [f]	0.998
K/Na 55-3	63	21.821	0.057	0.362	103.55	0.291	*1.002* [f]	
K/Na 55-4	71	21.873	0.095	0.355	101.22	0.466	*1.003* [f]	0.996
K/Na 55-5	71	21.809	0.245	0.366	104.71	1.182	*1.001* [f]	
K/Na 55-6	74	21.639	0.343	0.37	102.23	1.635	*1.001* [f]	0.998
K/Na 55-7	71	21.445	0.5	0.396	121.46	2.821	0.999	
K/Na 55-8	70	22.072	0.773	0.368	101.59	3.529	*0.997* [f]	0.994
K/Na 55-9	72	20.841	1.128	0.399	99.908	5.327	0.992	
K/Na 55-10	66	19.906	2.434	0.369	96.451	11.638	*0.985* [f]	0.987
K/Na 55-11	75	18.16	4.421	0.365	82.965	20.145	*0.996* [f]	0.976
K/Na 55-12	59	15.67	6.118	0.34	74.646	28.844	*0.973* [f]	0.964
K/Na 55-13	61	13.757	8.807	0.371	64.169	40.408	*0.950* [f]	0.939
K/Na 55-14	48	9.958	12.436	0.36	47.611	56.684	*0.811* [f]	0.890
K/Na 55-15	58	8.737	13.384	0.371	43.027	60.931	*0.754* [f]	0.876
K/Na 55-16	66	6.818	15.188	0.395	34.690	69.059	*0.721* [f]	
K/Na 55-17	64	6.002	16.529	0.396	30.319	73.594	*0.695* [f]	0.808
K/Na 55-18	67	3.533	18.764	0.374	20.232	83.605	*0.587* [f]	0.700
K/Na 55-19	25	2.899	47.145	2.51	6.888	94.060	*0.296* [f]	0.510
K/Na 55-20	18	1.059	49.14	0.5	3.053	96.460	0.084	
K/Na 55-21	20	0	49.991	0.52	1.089	100.30	0.080	
K/Na 55-22	14	0	49.82	0.49	0.818	100.70	0.016	
K/Na 55-23	8	0	49.951	0.48	0.503	99.718	*-0.074* [f]	
K/Na 55-24	5	0	50.052	0.51	0.357	103.66	*-0.177* [f]	

[a] 71 days in oven, [b] concentration = 0.0995 mol/kg, [c] concentration = 0.0995 mol/kg, [d] uncorrected ICP data, [e] calculated from weight corrected aqueous cation concentrations according to equations (1), (3), and (5). [f] value not used in thermodynamic analyses.

Table 7. Experimental details and results of K/Sr exchange experiments at 55 °C[a]

sample id	K-heulandite (mg)	K-stock [b] (g of solution)	Sr-stock [c] (g of solution)	weight loss (g)	$m\mathrm{K}^{+}$ [d] mmol/kg	$m\mathrm{Sr}^{2+}$ [d] mmol/kg	X_{Sr} [e] calculated	X_{Sr} ICP
K/Sr 55-1	49.5	22.033	0.042	0.525	101.92	0.023	0.011	
K/Sr 55-2	57	23.045	0.068	0.553	102.38	0.036	0.016	
K/Sr 55-3	44	21.999	0.101	0.554	102.38	0.084	0.026	
K/Sr 55-4	40.5	22.064	0.167	0.565	101.70	0.173	0.040	
K/Sr 55-5	56	21.892	0.425	0.565	100.67	0.479	0.070	
K/Sr 55-6	46	21.723	0.617	0.548	100.35	0.851	0.100	
K/Sr 55-7	51	22.071	0.865	0.564	99.791	1.214	0.120	
K/Sr 55-8	46	21.41	1.373	0.555	98.622	2.238	0.166	
K/Sr 55-9	39	20.656	2.025	0.553	96.076	3.679	0.218	
K/Sr 55-10	40	19.899	3.669	0.552	89.757	6.938	*0.278* [f]	0.300
K/Sr 55-11	39	17.948	6.483	0.555	79.306	12.471	0.381	
K/Sr 55-12	49	16.827	9.606	0.54	71.141	17.553	0.430	
K/Sr 55-13	35	13.92	13.885	0.565	55.920	25.079	0.548	
K/Sr 55-14	40	9.828	16.245	0.566	43.390	31.280	0.559	
K/Sr 55-15	42	8.936	17.742	0.551	38.870	33.216	0.579	
K/Sr 55-16	47	6.716	18.464	0.557	32.270	36.354	0.586	
K/Sr 55-17	45	5.706	20.382	0.567	27.089	38.975	0.627	
K/Sr 55-18	44	3.351	19.998	0.569	19.836	42.918	0.664	
K/Sr 55-19	23	1.399	47.756	0.73	4.316	49.860	0.902	
K/Sr 55-20	21	0.488	49.847	0.72	2.181	50.390	0.887	
K/Sr 55-21	10	0	51.938	0.72	0.567	51.301	0.953	
K/Sr 55-22	7	0	52.22	0.72	0.389	51.157	0.934	
K/Sr 55-23	6	0	51.197	0.73	0.326	51.796	0.846	
K/Sr 55-24	4	0	56.5	0.71	0.246	51.859	*1.3307*[f]	

[a] 70 days in oven, [b] concentration = 0.0995 mol/kg, [c] concentration = 0.0497 mol/kg, [d] uncorrected ICP data, [e] calculated from weight corrected aqueous cation concentrations according to equations (1), (3), and (5). [f] value not used in thermodynamic analyses.

Table 8. Experimental details and results of Na/Sr exchange experiments at 55 °C[a]

sample id	Na-heulandite (mg)	Na-stock [b] (g of solution)	Sr-stock [c] (g of solution)	weight loss (g)	$m\mathrm{Na}^{+}$ [d] mmol/kg	$m\mathrm{Sr}^{2+}$ [d] mmol/kg	X_{Sr} [e] calculated	X_{Sr} ICP
Na/Sr 55-1	57	30.012	0.024	0.544	102.02	0.001	*0.007* [f]	0.016
Na/Sr 55-2	52	29.914	0.027	0.561	101.71	0.003	0.008	
Na/Sr 55-3	72	29.981	0.041	0.551	102.03	0.003	*0.009* [f]	0.019
Na/Sr 55-4	68	30.078	0.055	0.563	100.84	0.004	0.013	
Na/Sr 55-5	68	29.951	0.164	0.567	100.12	0.004	*0.041* [f]	0.055
Na/Sr 55-6	60	29.825	0.232	0.561	98.450	0.009	*0.067* [f]	0.127
Na/Sr 55-7	49	29.973	0.327	0.555	96.770	0.016	*0.121* [f]	0.141
Na/Sr 55-8	82	29.401	0.546	0.559	98.320	0.014	0.123	
Na/Sr 55-9	47	29.457	0.809	0.571	98.960	0.209	*0.320* [f]	0.381
Na/Sr 55-10	67	28.45	1.561	0.564	93.870	0.603	*0.417* [f]	0.475
Na/Sr 55-11	59	26.985	3.037	0.57	93.030	3.021	*0.518* [f]	0.608
Na/Sr 55-12	50	25.16	4.818	0.562	83.110	6.079	*0.495* [f]	
Na/Sr 55-13	51	23.308	6.67	0.531	80.890	9.298	*0.535* [f]	0.676
Na/Sr 55-14	55	18.928	11.033	0.563	67.830	16.390	*0.626* [f]	0.711
Na/Sr 55-15	46	17.616	12.786	0.556	60.130	19.366	*0.462* [f]	
Na/Sr 55-16	71	14.884	15.084	0.565	55.220	22.531	*0.612* [f]	0.734
Na/Sr 55-17	50	13.559	16.122	0.564	47.460	25.729	*0.292* [f]	
Na/Sr 55-18	48	9.453	20.773	0.561	36.330	33.453	*0.696* [f]	0.748
Na/Sr 55-19	29	6.907	43.757	0.55	16.250	43.475	*1.593* [f]	
Na/Sr 55-20	21	3.579	46.506	0.54	8.323	47.229	*0.606* [f]	
Na/Sr 55-21	15	0	50.031	0.54	0.946	51.620	*1.026* [f]	
Na/Sr 55-22	13	0	49.985	0.55	0.783	51.100	0.954	
Na/Sr 55-23	10	0	49.881	0.57	0.632	51.963	*1.017* [f]	
Na/Sr 55-24	7	0	49.955	0.57	0.457	51.170	*1.130* [f]	
Na/Sr 55-25	18	0	222.82	1.72	0.272	51.837	*1.183* [f]	
Na/Sr 55-26	16	0	184.47	1.78	0.261	52.012	0.932	
Na/Sr 55-27	9.5	0	205.37	1.77	0.152	51.431	*1.145* [f]	

[a] 78 days in oven, [b] concentration = 0.0994 mol/kg, [c] concentration = 0.0496 mol/kg, [d] uncorrected ICP data, [e] calculated from weight corrected aqueous cation concentrations according to equations (1), (3), and (5). [f] value not used in thermodynamic analyses.

Table 9. Experimental details and results of Ca/K exchange experiments at 85 °C[a]

sample id	Ca-heulandite (mg)	Ca-stock [b] (g of solution)	K-stock [c] (g of solution)	weight loss (g)	$m\mathrm{Ca}^{2+}$ [d] mmol/kg	$m\mathrm{K}^{+}$ [d] mmol/kg	X_{Ca} [e] calculated	X_{Ca} ICP
Ca/K 85-1	41	25.101	0.073	1.071	47.570	0.200	0.966	
Ca/K 85-2	40.5	24.726	0.253	1.072	47.300	0.794	0.925	
Ca/K 85-3	51.5	24.736	0.122	1.076	47.556	0.434	0.988	
Ca/K 85-4	46	24.779	0.448	1.088	46.829	1.448	*0.908* [f]	
Ca/K 85-5	57	23.962	0.94	1.03	46.287	3.271	*0.895* [f]	0.791
Ca/K 85-6	51	23.208	1.515	1.07	45.444	5.735	*0.935* [f]	0.757
Ca/K 85-7	58	21.748	2.918	1.091	43.206	11.457	*0.960* [f]	0.673
Ca/K 85-8	45	20.506	4.021	1.099	41.103	16.589	*1.153* [f]	0.639
Ca/K 85-9	48	16.769	9.106	1.123	31.990	35.684	*1.241* [f]	0.500
Ca/K 85-10	48	10.234	14.909	1.049	21.597	62.359	*0.912* [f]	0.373
Ca/K 85-11	51	4.982	19.6	1.123	11.981	83.342	*0.484* [f]	0.251

[a] 25 days in oven, [b] concentration = 0.0500 mol/kg, [c] concentration = 0.1001 mol/kg, [d] uncorrected ICP data, [e] calculated from weight corrected aqueous cation concentrations according to equations (1), (3), and (5). [f] value not used in thermodynamic analyses.

Table 10. Experimental details and results of K/Ca exchange experiments at 85 °C[a]

sample id	K-heulandite (mg)	Ca-stock [b] (g of solution)	K-stock [c] (g of solution)	weight loss (g)	$m\mathrm{Ca}^{2+}$ [d] mmol/kg	$m\mathrm{K}^{+}$ [d] mmol/kg	X_{Ca} [e] calculated	X_{Ca} ICP
K/Ca 85-1	38	24.125	0.492	1.075	0.793	103.11	0.057	
K/Ca 85-2	39	25.254	0.194	1.05	0.257	103.95	0.031	
K/Ca 85-3	34	23.86	0.916	1.035	1.562	101.98	0.100	
K/Ca 85-4	36	22.979	1.539	1.077	2.784	99.320	0.128	
K/Ca 85-5	35	22.21	2.354	1.022	4.378	96.266	0.177	
K/Ca 85-6	38	19.994	4.904	1.077	9.975	94.470	*0.342* [f]	
K/Ca 85-7	42	16.943	7.588	1.036	15.048	76.334	*0.364* [f]	0.273
K/Ca 85-8	43	14.077	10.477	1.077	20.781	64.482	*0.519* [f]	
K/Ca 85-9	42	9.608	15.371	1.066	33.065	48.439	*0.641* [f]	0.447
K/Ca 85-10	42	4.747	20.4	0.892	39.462	23.775	*0.788* [f]	

[a] 25 days in oven, [b] concentration = 0.1001 mol/kg, [c] concentration = 0.0500 mol/kg, [d] uncorrected ICP data, [e] calculated from weight corrected aqueous cation concentrations according to equations (1), (3), and (5). [f] value not used in thermodynamic analyses.

Table 11. Experimental details and results of K/Sr exchange experiments at 85 °C[a]

sample id	K-heulandite (mg)	K-stock [b] (g of solution)	Sr-stock [c] (g of solution)	weight loss (g)	$m\mathrm{K}^{+}$ [d] mmol/kg	$m\mathrm{Sr}^{2+}$ [d] mmol/kg	X_{Sr} [e] calculated	X_{Sr} ICP
K/Sr 85-1	47	29.836	0.176	0.724	102.47	0.084	0.049	
K/Sr 85-2	48	29.416	0.683	0.785	100.65	0.598	0.134	
K/Sr 85-3	39	28.348	1.52	0.816	98.586	1.877	0.230	
K/Sr 85-4	41	27.62	2.153	0.824	97.056	2.794	0.287	
K/Sr 85-5	34	27.018	3.067	0.879	94.597	4.374	0.357	
K/Sr 85-7	39	20.946	8.893	0.903	76.490	14.382	0.481	
K/Sr 85-8	54	17.703	12.632	0.793	65.471	20.169	*0.514* [f]	0.507
K/Sr 85-10	48	7.516	22.533	0.846	30.727	37.435	0.784	
K/Sr 85-11	32	4.817	25.42	0.873	19.826	42.610	*0.915* [f]	0.720
K/Sr 85-12	23	1.461	28.795	0.904	7.332	48.524	0.987	
K/Sr 85-14	19	0.438	49.616	7.442	2.096	51.396	0.966	
K/Sr 85-15	13	0	50.766	1.33	0.866	52.019	*1.249* [f]	

[a] 20 days in oven, [b] concentration = 0.1001 mol/kg, [c] concentration = 0.0500 mol/kg, [d] uncorrected ICP data, [e] calculated from weight corrected aqueous cation concentrations according to equations (1), (3), and (5). [f] value not used in thermodynamic analyses.

Table 12. Experimental details and results of Na/Ca exchange experiments at 85 °C[a]

sample id	Na-heulandite (mg)	Ca-stock [b] (g of solution)	Na-stock [c] (g of solution)	weight loss (g)	$m\mathrm{Ca}^{2+}$ [d] mmol/kg	$m\mathrm{Na}^{+}$ [d] mmol/kg	X_{Ca} [e] calculated	X_{Ca} ICP
Na/Ca 85-1	43	0.043	29.152	0.704	0.016	104.46	0.014	
Na/Ca 85-2	48	0.119	29.166	0.817	0.030	105.16	0.038	
Na/Ca 85-3	44	0.212	29.351	0.871	0.035	104.54	0.081	
Na/Ca 85-4	45	0.578	29.347	0.702	0.167	103.72	0.224	
Na/Ca 85-5	45	1.274	28.634	0.831	0.891	102.35	0.407	
Na/Ca 85-6	41	4.285	25.159	0.905	6.122	94.459	*0.608*[f]	0.594
Na/Ca 85-7	66	2.007	27.899	0.723	1.454	102.51	*0.441*[f]	0.456
Na/Ca 85-8	63	7.514	25.668	0.868	10.649	85.800	*0.331*[f]	0.645
Na/Ca 85-9	56	11.693	17.681	0.92	19.130	69.273	*0.612*[f]	0.714
Na/Ca 85-10	44	14.955	14.95	0.739	24.935	56.445	*0.566*[f]	0.743
Na/Ca 85-11	48	18.221	11.625	0.871	30.741	46.332	*0.750*[f]	0.778
Na/Ca 85-12	46	22.016	7.84	0.946	37.937	32.704	0.751	
Na/Ca 85-13	48	24.552	5.478	0.898	41.657	23.952	0.778	
Na/Ca 85-14	62	25.764	4.098	0.966	43.562	20.660	0.813	
Na/Ca 85-15	75	27.392	2.438	0.988	46.277	16.213	0.843	
Na/Ca 85-16	40	28.506	1.667	0.904	48.583	9.691	*0.841*[f]	0.873
Na/Ca 85-17	44	29.937	0.524	1.02	50.376	7.075	*1.338*[f]	0.884
Na/Ca 85-18	66	29.442	0.124	1.035	50.802	6.041	*0.659*[f]	0.888
Na/Ca 85-19	42	46.027	0.512	1.34	51.876	3.824	0.867	
Na/Ca 85-20	27	44.642	0.026	1.317	52.442	1.862	0.909	
Na/Ca 85-24	8	53.445	0	1.54	52.557	0.459	0.984	

[a] 19 days in oven, [b] concentration = 0.0500 mol/kg, [c] concentration = 0.0998 mol/kg, [d] uncorrected ICP data, [e] calculated from weight corrected aqueous cation concentrations according to equations (1), (3), and (5). [f] value not used in thermodynamic analyses.

Table 13. Experimental details and results of Na/K exchange experiments at 85 °C[a]

sample id	Na-heulandite (mg)	K-stock [b] (g of solution)	Na-stock [c] (g of solution)	weight loss (g)	$m\mathrm{K}^{+}$ [d] mmol/kg	$m\mathrm{Na}^{+}$ [d] mmol/kg	X_{K} [e] calculated	X_{K} ICP
Na/K 85-1	41.5	0.025	29.648	0.751	0.063	102.92	0.006	
Na/K 85-2	62	0.05	29.728	0.748	0.093	102.27	0.012	
Na/K 85-3	55.5	0.115	29.308	0.759	0.183	101.54	0.038	
Na/K 85-4	39	0.303	29.941	0.769	0.556	101.37	0.119	
Na/K 85-5	62	0.61	29.229	0.752	1.018	100.99	0.170	
Na/K 85-6	52	1.072	28.84	0.734	2.333	100.20	0.254	
Na/K 85-7	44	2.763	26.915	0.743	7.540	95.692	*0.459* [f]	0.495
Na/K 85-8	52	5.349	24.588	0.676	15.834	86.705	*0.475* [f]	0.634
Na/K 85-9	60	7.833	21.816	0.653	23.420	79.691	0.622	
Na/K 85-10	50	10.808	18.911	0.606	33.723	68.920	0.712	
Na/K 85-11	44	15.711	14.48	0.592	49.882	53.626	0.900	
Na/K 85-12	43	17.862	12.066	0.633	56.508	44.745	0.919	
Na/K 85-13	42	19.775	10.162	0.798	63.535	39.405	*1.051* [f]	0.937
Na/K 85-14	43	20.959	9.183	0.822	67.625	36.252	*1.056* [f]	0.947
Na/K 85-15	55	24.806	5.709	0.826	77.926	25.253	*1.083* [f]	0.966
Na/K 85-16	44	26.26	3.748	0.819	88.227	17.980	*1.025* [f]	0.979
Na/K 85-17	32	28.789	1.256	0.813	96.241	7.596	*0.994* [f]	0.991
Na/K 85-18	30	28.223	1.967	0.776	94.242	9.759	0.976	
Na/K 85-19	27	49.472	1.732	2.11	98.234	5.227	*1.071* [f]	0.991
Na/K 85-20	20	49.11	0.676	1.08	100.51	2.786	*1.125* [f]	0.993
Na/K 85-21	20	48.157	0	1.1	101.53	1.503	*1.183* [f]	0.996
Na/K 85-22	18	48.218	0	1.027	102.26	1.407	*1.224* [f]	0.996
Na/K 85-24	5	48.098	0	1.032	103.40	0.486	*1.515* [f]	

[a] 21 days in oven, [b] concentration = 0.1001 mol/kg, [c] concentration = 0.0998 mol/kg, [d] uncorrected ICP data, [e] calculated from weight corrected aqueous cation concentrations according to equations (1), (3), and (5). [f] value not used in thermodynamic analyses.

Table 14. Experimental details and results of Na/Sr exchange experiments at 85 °C[a]

sample id	Na-heulandite (mg)	Na-stock [b] (g of solution)	Sr-stock [c] (g of solution)	weight loss (g)	$m\mathrm{Na}^{+}$ [d] mmol/kg	$m\mathrm{Sr}^{2+}$ [d] mmol/kg	X_{Sr} [e] calculated	X_{Sr} ICP
Na/Sr 55-1	61	29.866	0.045	1.011	107.33	0.007	0.012	
Na/Sr 55-2	45	30.211	0.202	0.986	106.20	0.007	0.080	
Na/Sr 55-3	54	29.772	0.3	1.079	106.12	0.014	0.100	
Na/Sr 55-4	45	29.475	0.675	1.066	106.38	0.061	0.315	
Na/Sr 55-5	45	28.917	1.154	1.07	106.47	0.413	*0.527* [f]	0.539
Na/Sr 55-6	44	27.747	2.013	1.029	96.110	1.707	*0.613* [f]	0.672
Na/Sr 55-7	55	24.41	5.346	0.925	88.700	6.689	*0.799* [f]	0.766
Na/Sr 55-8	52	21.103	8.722	0.981	71.920	13.049	*0.343* [f]	0.801
Na/Sr 55-9	50	18.045	11.965	0.961	64.130	18.182	*0.602* [f]	0.819
Na/Sr 55-10	54	14.289	15.95	0.946	54.740	24.835	*0.965* [f]	0.834
Na/Sr 55-11	63	9.396	20.396	0.937	37.820	32.562	*0.713* [f]	0.864
Na/Sr 55-12	47	7.569	22.708	0.928	28.890	36.925	*0.518* [f]	0.869
Na/Sr 55-13	49	5.76	24.682	0.947	25.520	39.694	*1.312* [f]	0.877
Na/Sr 55-14	50	4.707	25.416	0.99	21.260	41.483	*0.945* [f]	0.890
Na/Sr 55-15	48	2.42	27.723	1.013	12.820	45.728	*0.825* [f]	0.909
Na/Sr 55-16	49	28.71	1.186	1.039	99.310	0.406	*0.480* [f]	0.527
Na/Sr 55-17	37	0.523	29.568	1.06	5.886	50.567	*1.063* [f]	
Na/Sr 55-18	31	0.427	29.899	1.023	4.809	51.319	*1.022* [f]	
Na/Sr 55-19	23	0.474	50.179	1.32	2.336	51.940	*0.883* [f]	
Na/Sr 55-22	14	0	46.454	1.231	1.009	53.109	*1.106* [f]	
Na/Sr 55-23	11	0	46.529	1.58	0.763	52.064	*1.074* [f]	
Na/Sr 55-24	7	0	54.45	1.11	0.456	52.203	*1.319* [f]	

[a] 21 days in oven, [b] concentration = 0.0500 mol/kg, [c] concentration = 0.0998 mol/kg, [d] uncorrected ICP data, [e] calculated from weight corrected aqueous cation concentrations according to equations (1), (3), and (5). [f] value not used in thermodynamic analyses.

Table 15. Summary of thermodynamic results

Isotherm	A	B	Exchange reaction	ln*K*	W_{A-B} (J mol^{-1} K^{-1})	W_{B-A} (J mol^{-1} K^{-1})
Ca/Na 55, Na/Ca 55	Ca	Na	$2\ Na^+ + CaZ_2 \bullet 6.24H_2O = Ca^{2+} + 2\ NaZ \bullet 2.73H_2O + 0.78\ H_2O$	-1.30 ± 0.16	560 ± 940	10,426 ± 272
K/Ca 55	Ca	K	$2\ K^+ + CaZ_2 \bullet 6.24H_2O = Ca^{2+} + 2\ KZ \bullet 2.27H_2O + 1.70\ H_2O$	2.95 ± 0.23	6,995 ± 648	1,234 ± 1,992
K/Na 55	K	Na	$Na^+ + KZ \bullet 2.27H_2O + 0.46\ H_2O = K^+ + NaZ \bullet 2.73H_2O$	-2.11 ± 0.55	-1,582 ± 980	-368 ± 1,498
K/Sr 55	Sr	K	$2\ K^+ + SrZ_2 \bullet 2n_{Sr}H_2O = Sr^{2+} + 2\ KZ \bullet 2n_KH_2O + 2(n_{Sr}-n_K)\ H_2O$[a]	0.38 ± 0.13	6,171 ± 372	3,481 ± 1,485
Na/Sr 55	Sr	Na	$2\ Na^+ + SrZ_2 \bullet 2n_{Sr}H_2O = Sr^{2+} + 2\ NaZ \bullet 2n_{Na}H_2O + 2(n_{Sr}-n_{Na})\ H_2O$[b]	-3.17 ± 0.16	1,711 ± 753	11,540 ± 623
Ca/K 85, K/Ca 85	Ca	K	$2\ K^+ + CaZ_2 \bullet 6.06H_2O = Ca^{2+} + 2\ KZ \bullet 2.16H_2O + 1.74\ H_2O$	2.05 ± 0.12	3,774 ± 653	7,485 ± 498
K/Sr 85	Sr	K	$2\ K^+ + SrZ_2 \bullet 2n_{Sr}H_2O = Sr^{2+} + 2\ KZ \bullet 2n_KH_2O + 2(n_{Sr}-n_K)\ H_2O$[a]	-0.53 ± 0.29	7,770 ± 1,550	2,703 ± 967
Na/Ca 85	Ca	Na	$2\ Na^+ + CaZ_2 \bullet 6.06H_2O = Ca^{2+} + 2\ NaZ \bullet 2.63H_2O + 0.80\ H_2O$	-2.08 ± 0.23	444 ± 1,100	9,519 ± 368
Na/K 85	K	Na	$Na^+ + KZ \bullet 2.16H_2O + 0.47\ H_2O = K^+ + NaZ \bullet 2.63H_2O$	-2.53 ± 0.11	1,908 ± 1,100	1,112 ± 339
Na/Sr 85	Sr	Na	$2\ Na^+ + SrZ_2 \bullet 2n_{Sr}H_2O = Sr^{2+} + 2\ NaZ \bullet 2n_{Na}H_2O + 2(n_{Sr}-n_{Na})\ H_2O$[b]	-4.02 ± 0.35	-2,038 ± 1,703	7,745 ± 510

[a] n_{Sr} and n_K refer to the water content of homoionic Sr- and K-heulandites per charge equivalent, respectively, at the experimental temperature.
[b] n_{Sr} and n_{Na} refer to the water content of homoionic Sr- and Na-heulandites per charge equivalent, respectively, at the experimental temperature.

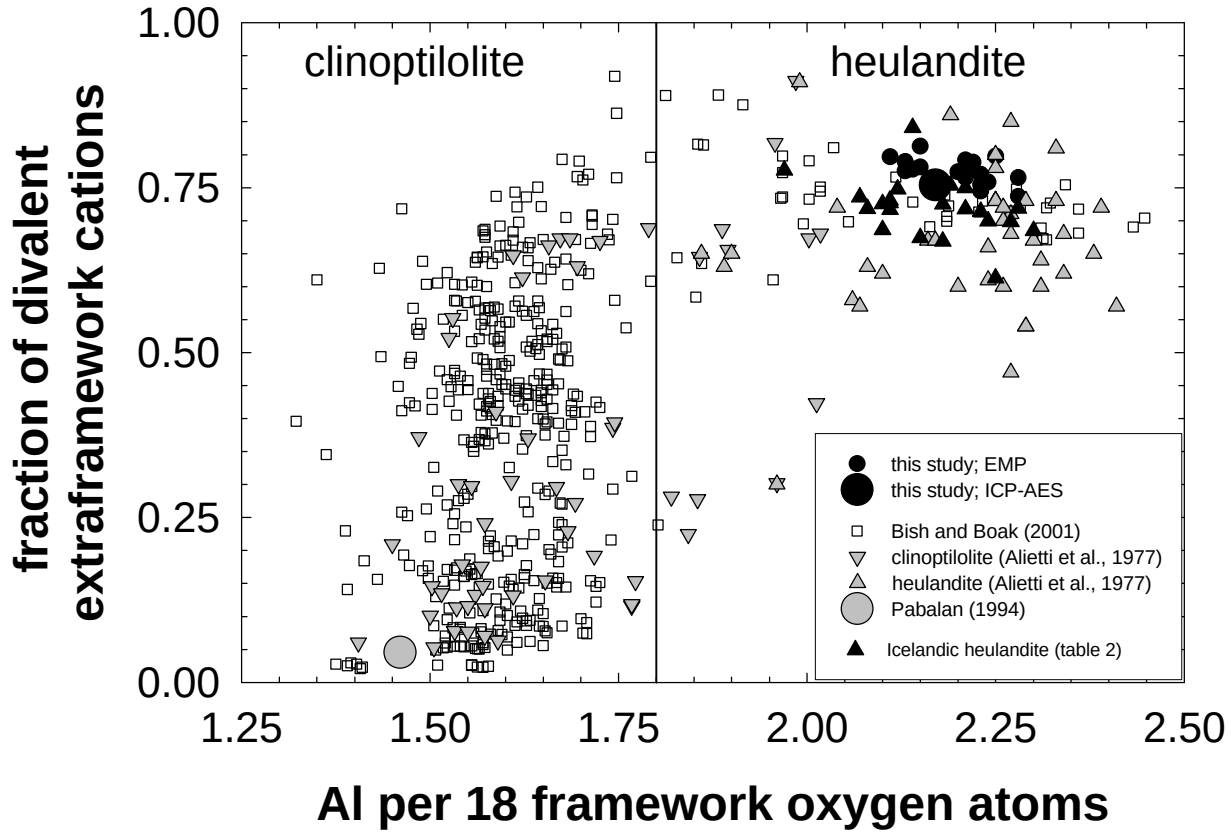
clinoptilolite
heulandite
fraction of divalent extraframework cations
Al per 18 framework oxygen atoms
1.00
0.75
0.50
0.25
0.00
1.25
1.50
1.75
2.00
2.25
2.50
this study; EMP
this study; ICP-AES
Bish and Boak (2001)
clinoptilolite (Alietti et al., 1977)
heulandite (Alietti et al., 1977)
Pabalan (1994)
Icelandic heulandite (table 2)

Figure 1

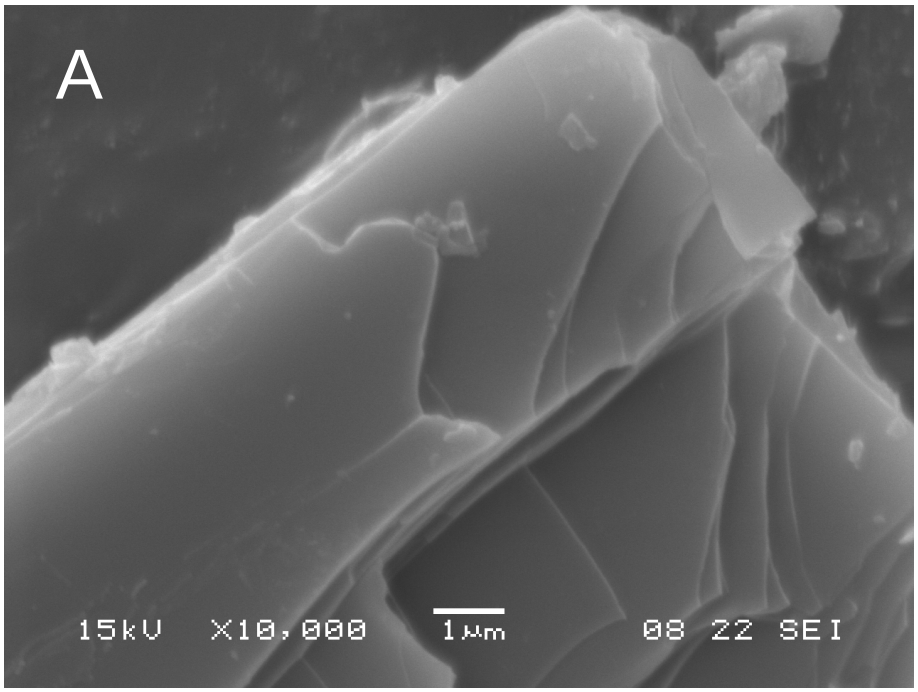

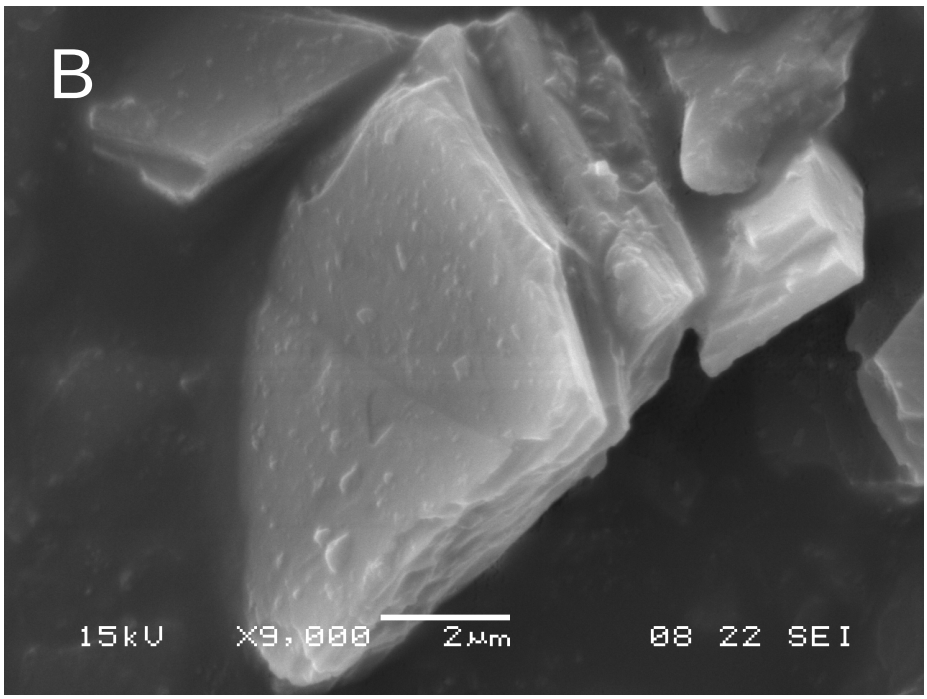

Figure 2

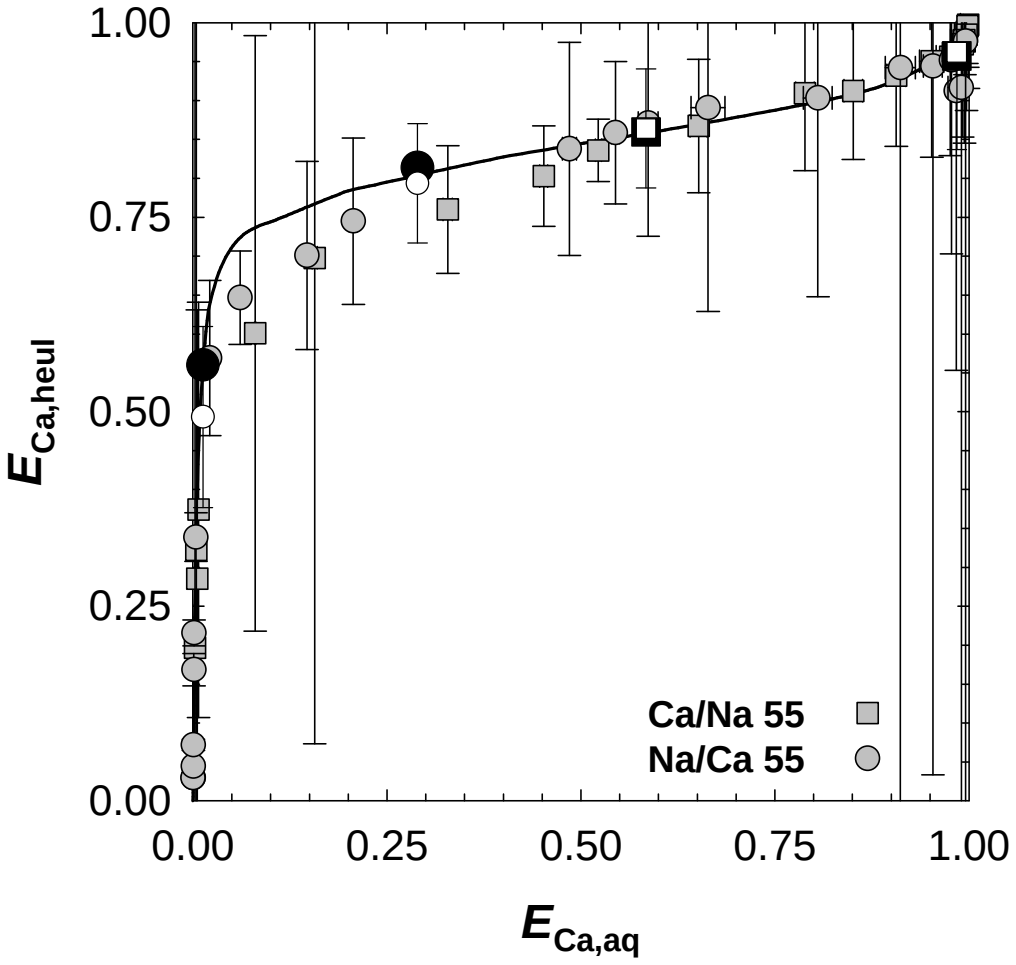
1.00
0.75
0.50
0.25
0.00
0.00
0.25
0.50
0.75
1.00
$E_{Ca,heul}$
$E_{Ca,aq}$
Ca/Na 55
Na/Ca 55

Figure 3

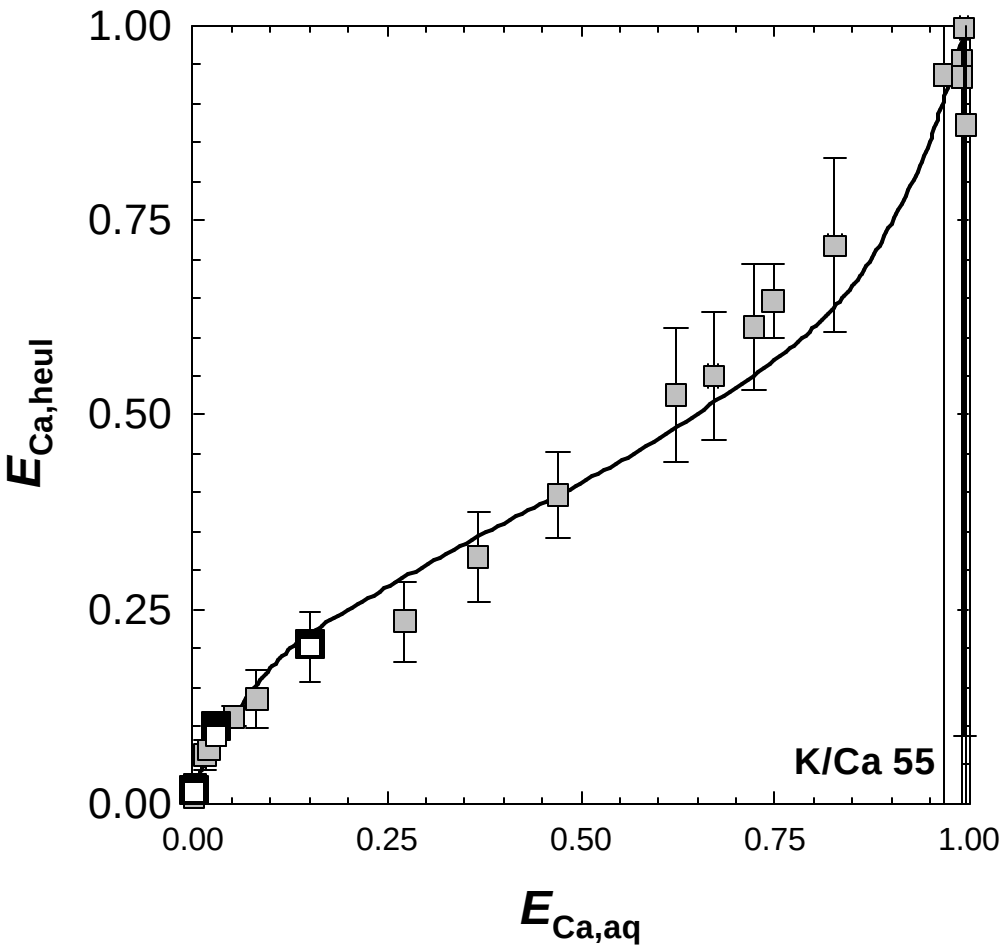

Figure 4

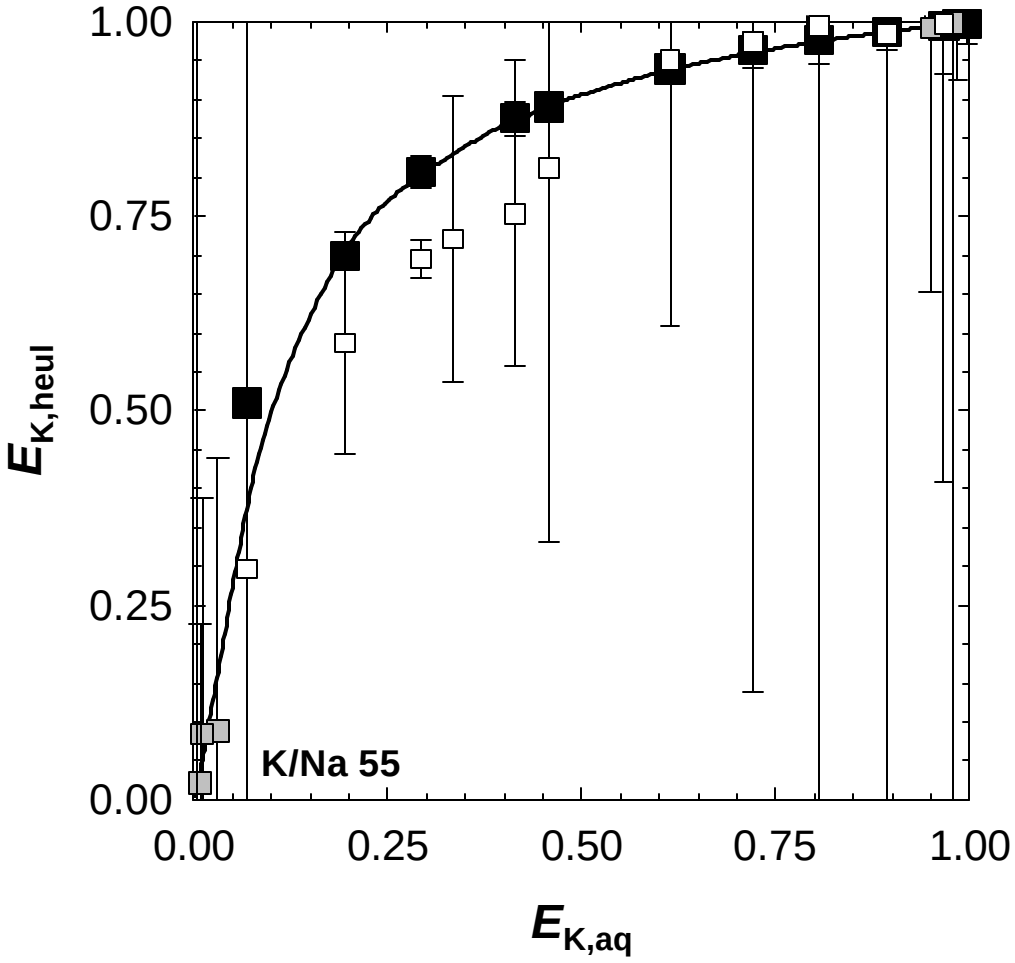

Figure 5

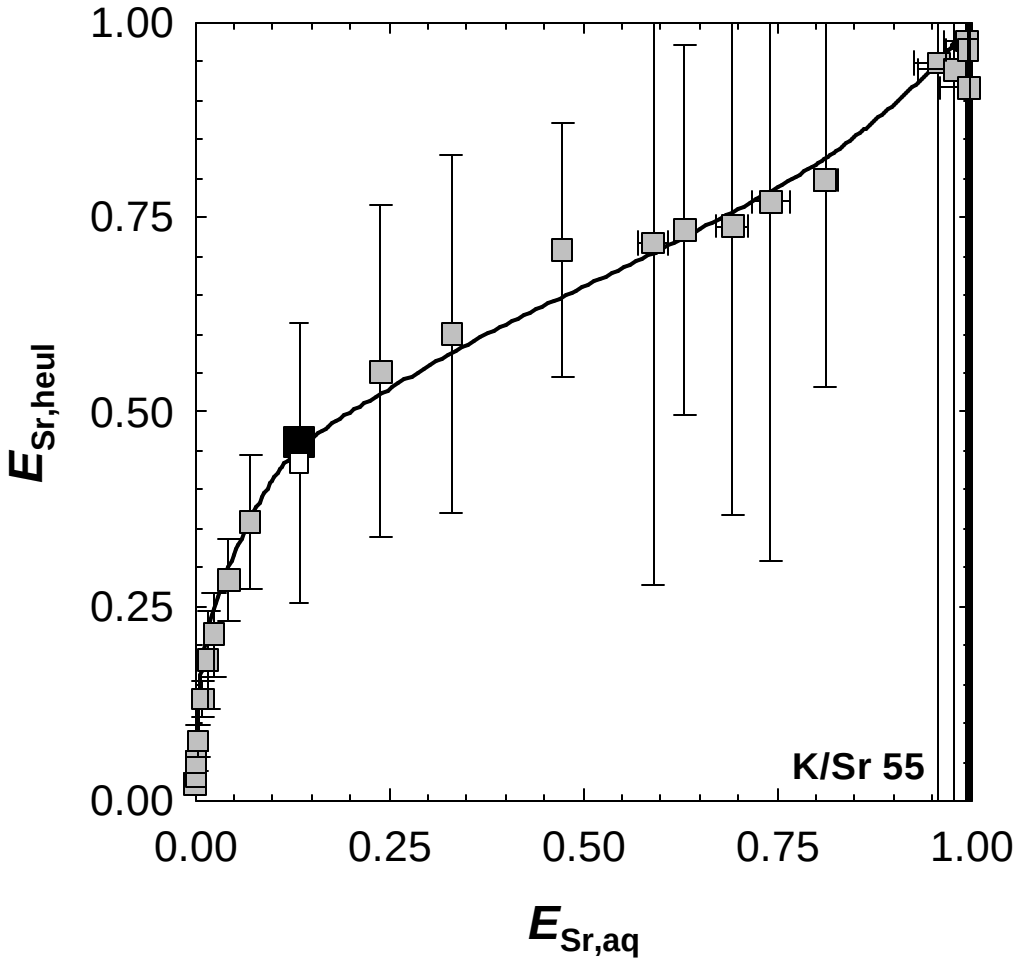

Figure 6

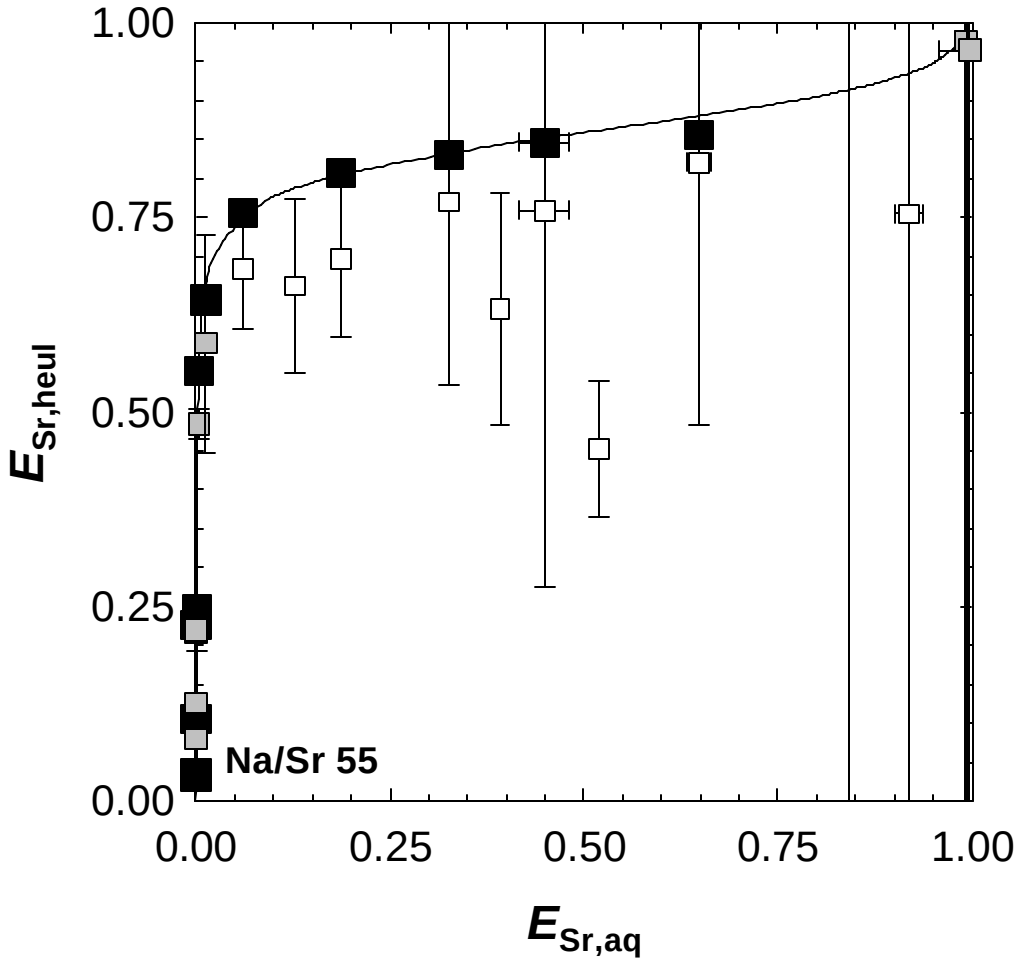

Figure 7

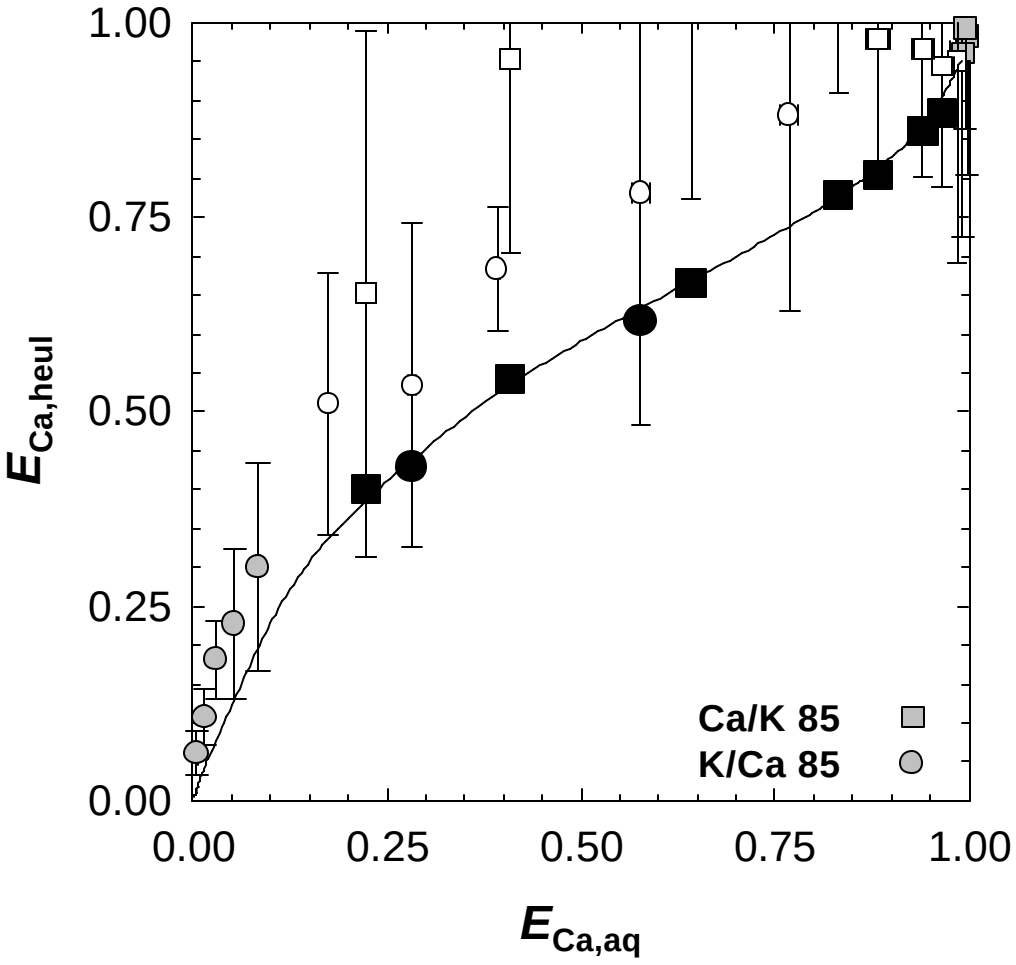
1.00
0.75
0.50
0.25
0.00
0.00
0.25
0.50
0.75
1.00
$E_{Ca,heul}$
$E_{Ca,aq}$
Ca/K 85
K/Ca 85

Figure 8

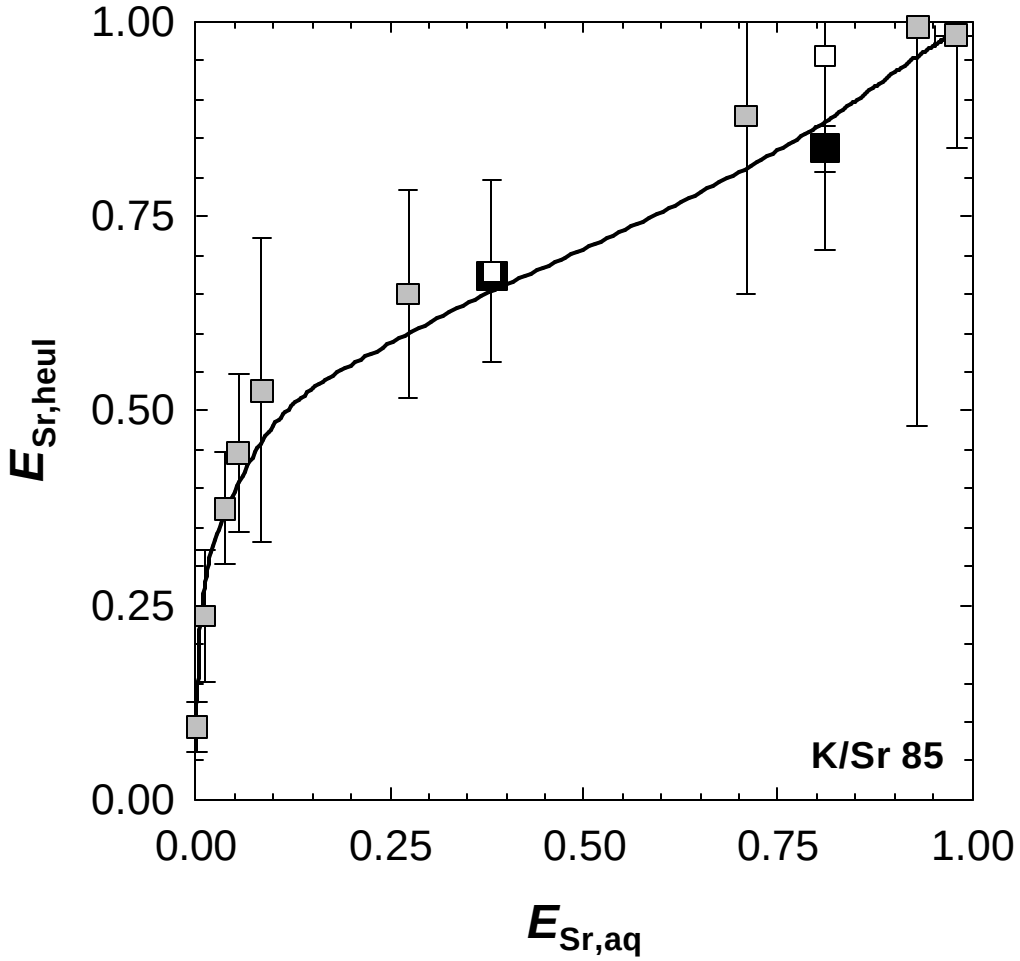

Figure 9

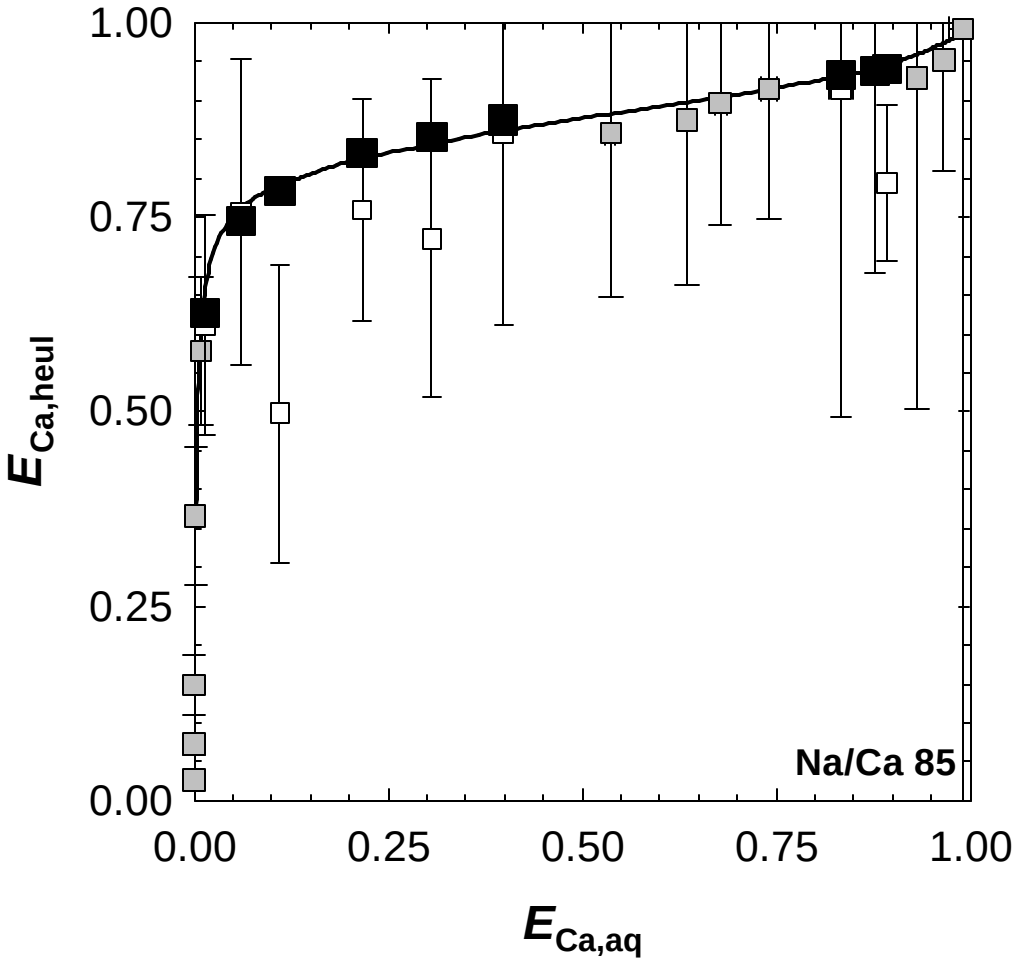

Figure 10

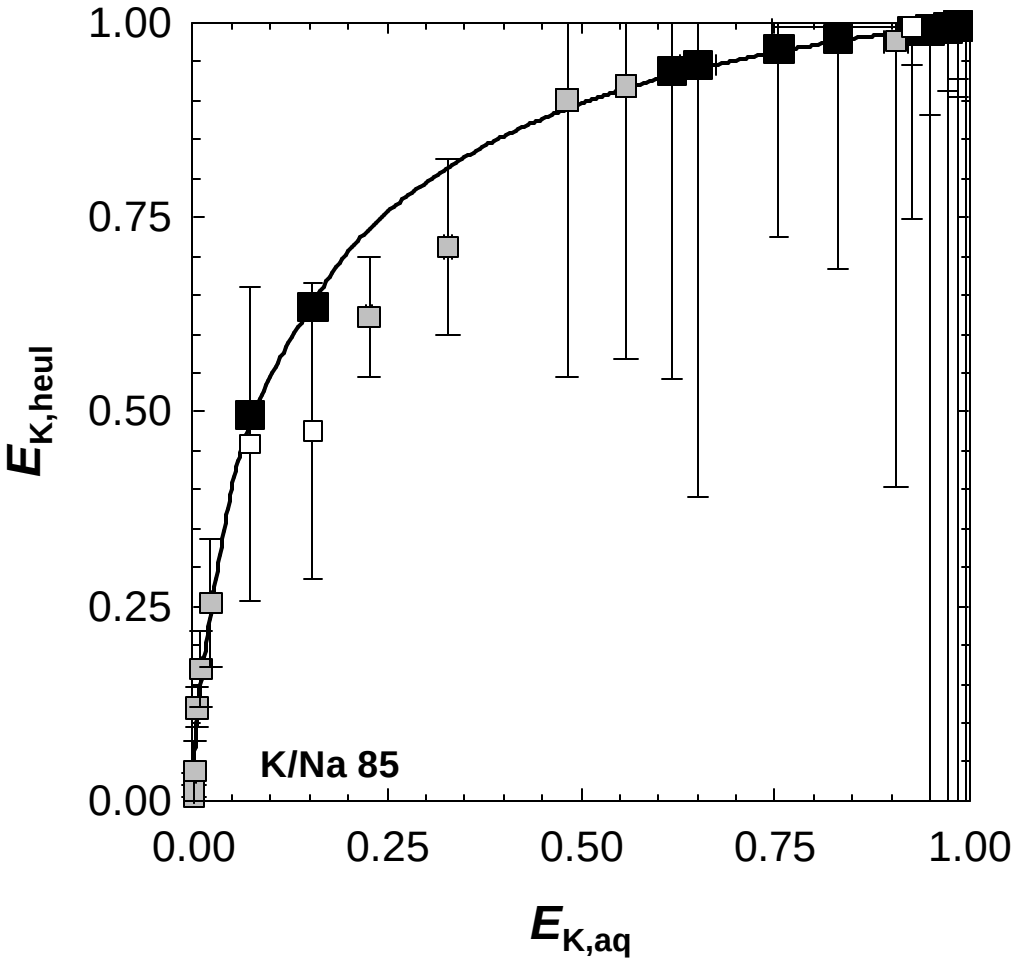

Figure 11

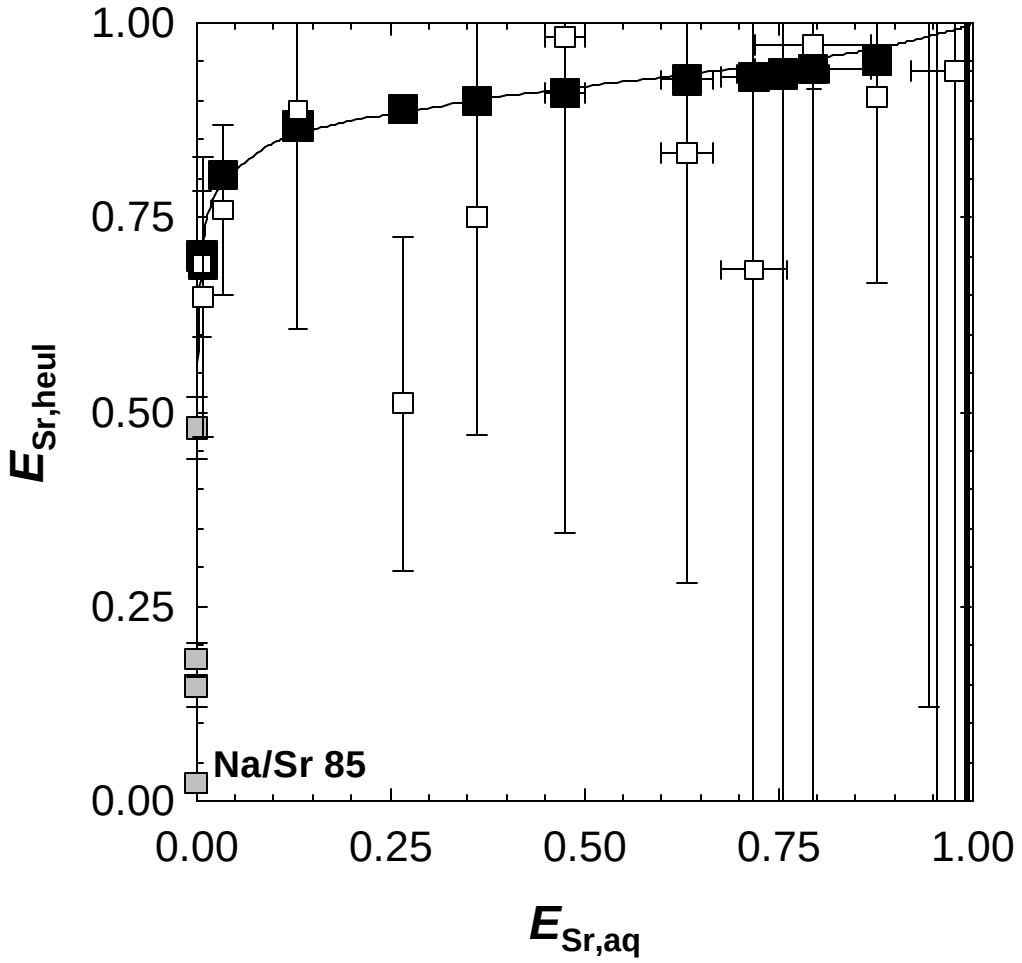

Figure 12

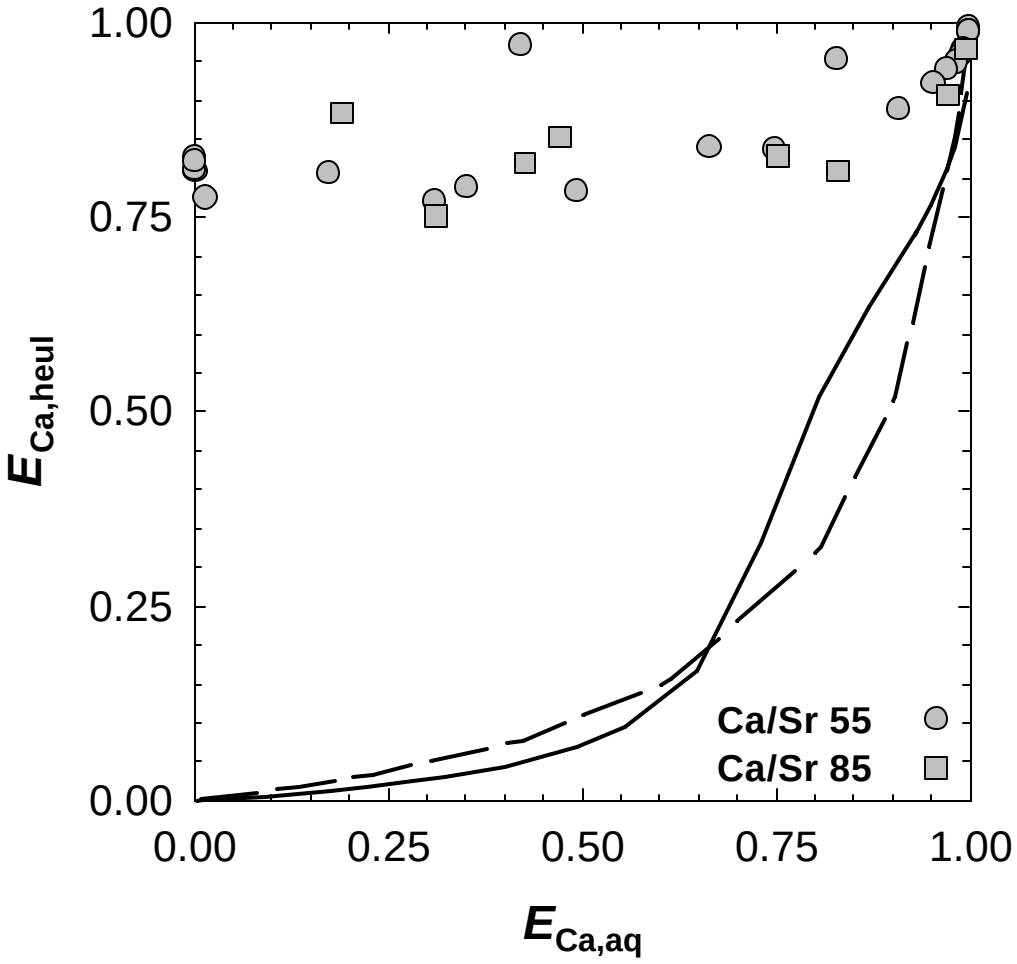
1.00
0.75
0.50
0.25
0.00
0.00
0.25
0.50
0.75
1.00
$E_{Ca,heul}$
$E_{Ca,aq}$
Ca/Sr 55
Ca/Sr 85

Figure 13

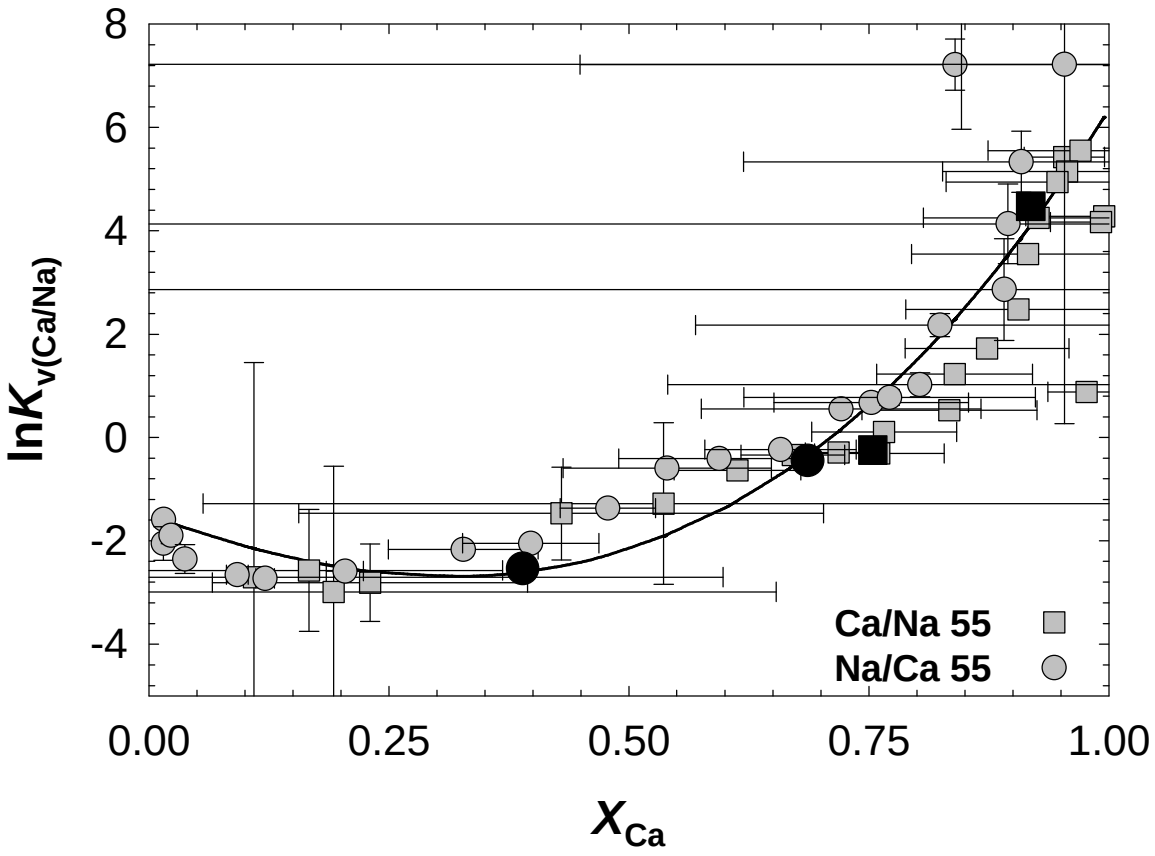

Figure 14

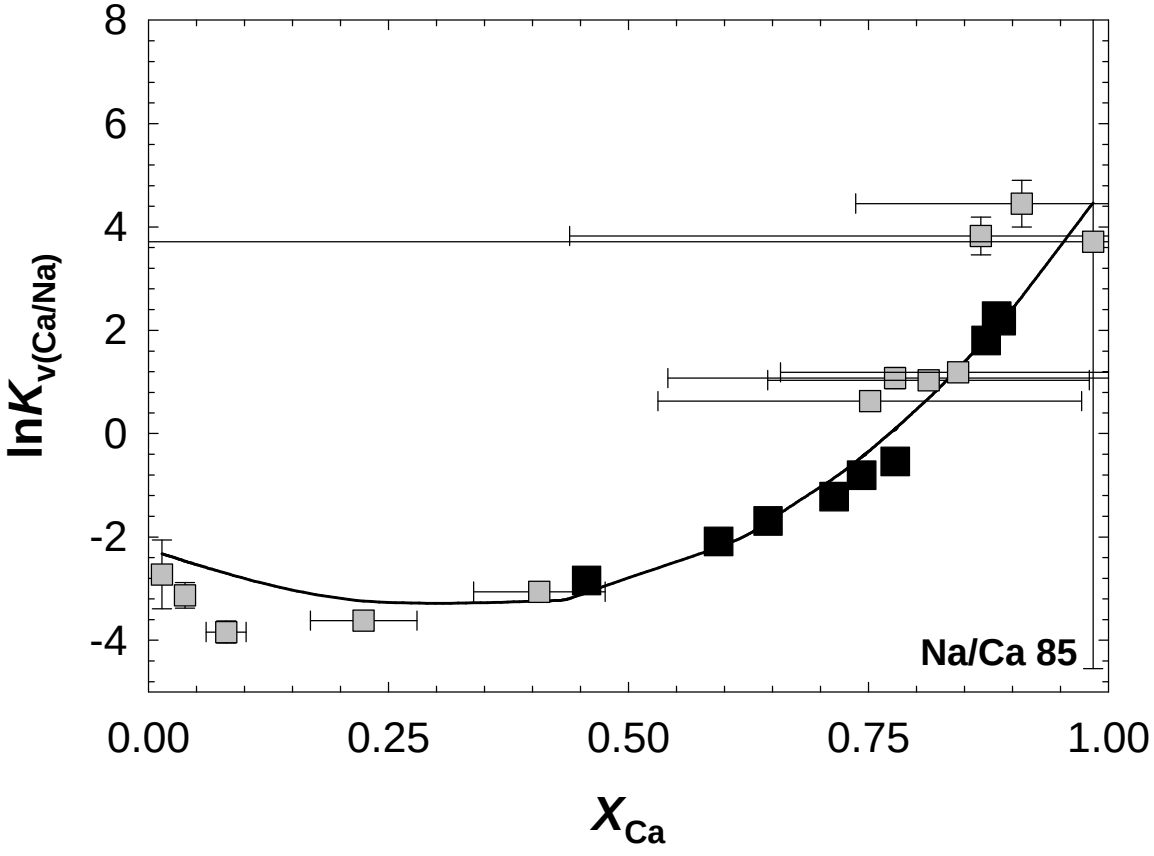

Figure 15

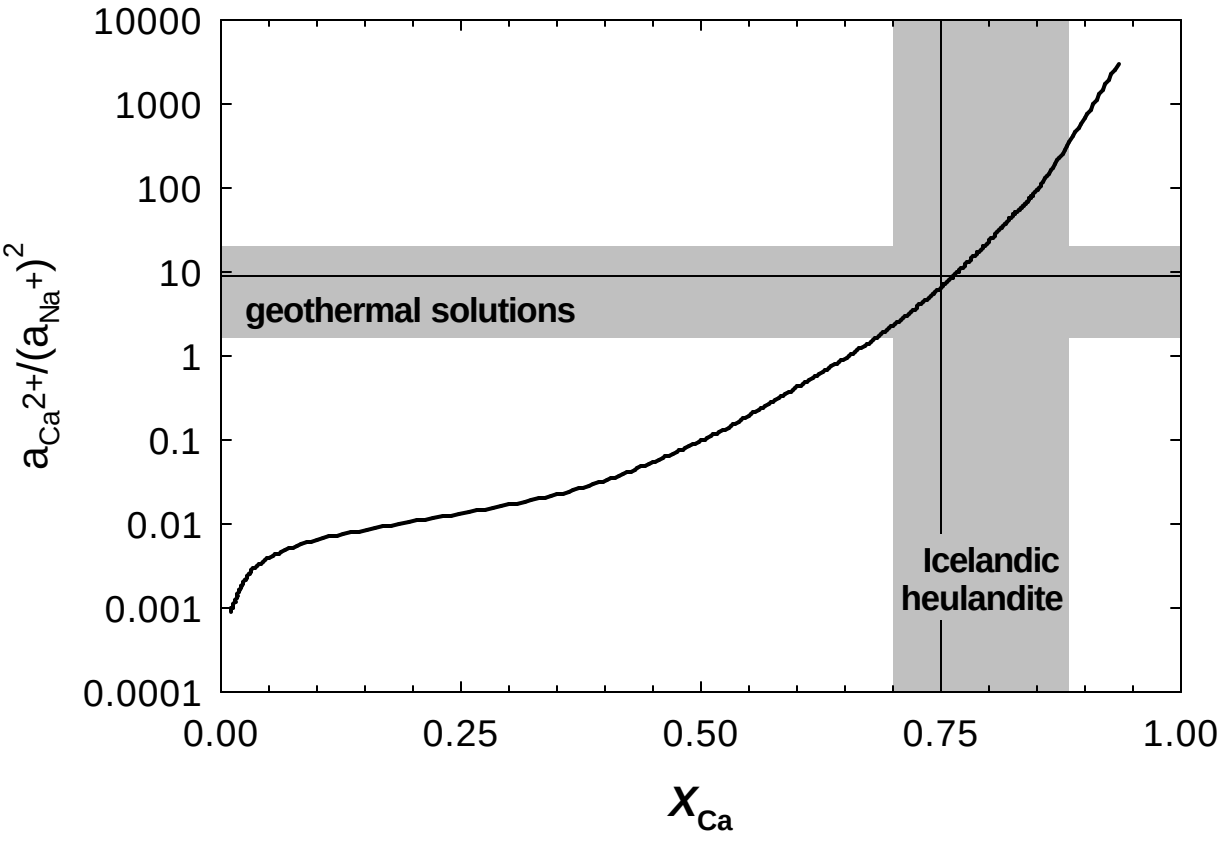
10000
1000
100
10
1
0.1
0.01
0.001
0.0001
0.00
0.25
0.50
0.75
1.00
$a_{Ca}^{2+}/(a_{Na}^{+})^2$
X_{Ca}
geothermal solutions
Icelandic
heulandite

Figure 16